Biomineralization: integrating mechanism and evolutionary history.

Pupa U.P.A. Gilbert, Kristin D. Bergmann, Nicholas Boekelheide, Sylvie Tambutté, Tali Mass, Frédéric Marin, Jess F. Adkins, Jonathan Erez, Benjamin Gilbert, Vanessa Knutson, et al.

Science Advances

11 MARCH 2022

AAAS

BIOPHYSICS

Biomineralization: Integrating mechanism and evolutionary history

Pupa U. P. A. Gilbert[1,2]*†, Kristin D. Bergmann[3], Nicholas Boekelheide[3], Sylvie Tambutté[4], Tali Mass[5], Frédéric Marin[6], Jess F. Adkins[7], Jonathan Erez[8], Benjamin Gilbert[9,10], Vanessa Knutson[11], Marjorie Cantine[3,12], Javier Ortega Hernández[11], Andrew H. Knoll[11]*

Calcium carbonate ($CaCO_3$) biomineralizing organisms have played major roles in the history of life and the global carbon cycle during the past 541 Ma. Both marine diversification and mass extinctions reflect physiological responses to environmental changes through time. An integrated understanding of carbonate biomineralization is necessary to illuminate this evolutionary record and to understand how modern organisms will respond to 21st century global change. Biomineralization evolved independently but convergently across phyla, suggesting a unity of mechanism that transcends biological differences. In this review, we combine $CaCO_3$ skeleton formation mechanisms with constraints from evolutionary history, omics, and a meta-analysis of isotopic data to develop a plausible model for $CaCO_3$ biomineralization applicable to all phyla. The model provides a framework for understanding the environmental sensitivity of marine calcifiers, past mass extinctions, and resilience in 21st century acidifying oceans. Thus, it frames questions about the past, present, and future of $CaCO_3$ biomineralizing organisms.

INTRODUCTION

Minerals made by organisms are called biominerals (*1*), and their formation mechanisms are collectively termed biomineralization (*2*–*4*). A major innovation in the history of life, biomineralization transformed the functional biology, evolutionary trajectory, and biogeochemical impact of numerous clades among animals, plants, and protists. While predation likely played a major role in the evolution of biomineralized structures, a variety of other functions accrued, including locomotion, buoyancy, grinding, reproduction, and detection of gravity, magnetic fields, or light. Biominerals may even have multiple functions at once, such as calcium carbonate ($CaCO_3$) armors that also serve as lenses in chitons (*5*), microbial shields in ants (*6*), or detoxification in most phyla (*7*). The establishment of genetic recipes for complex functional biominerals from the same basic ingredients is a remarkable product of evolution.

Ever since $CaCO_3$ biomineralization became widespread, during the Cambrian (*8*, *9*) and Ordovician (*10*) radiations of marine animals and algae, it has played a major role in the carbon cycle (*11*), affecting and being affected by the ambient environment on geologic time scales (*12*, *13*). Because of their persistence in the fossil record, biominerals in general, and $CaCO_3$ biominerals in particular, provide a major archive of the evolutionary history of life and environments on Earth. Looking forward, $CaCO_3$ biomineralization is challenged, for some phyla more than others, by 21st century global change.

Phylogenetic evidence (Fig. 1) shows that biominerals appeared in the fossil record long after the different phyla had diverged from one another (*14*). Because the biomineralizing organisms in various phyla do not have a common ancestor that was itself biomineralizing, they must have evolved strategies to form carbonate biominerals independently (*15*). These strategies are remarkably similar in ingredients and recipes across phyla; therefore, they evolved convergently (*15*).

A mechanistic understanding of how organisms make $CaCO_3$ biominerals is essential for understanding the evolutionary record of $CaCO_3$ biomineralization, elucidating its consequences for Earth surface environments, and clarifying the sensitivity of $CaCO_3$ biomineralizers to both past and future environmental changes (*16*–*22*). Here, we attempt to unify all known $CaCO_3$ biomineralization mechanisms into a single model applicable to all phyla, emphasizing the commonalities across diverse and divergent species. We show that insights on $CaCO_3$ skeleton formation pathway (*15*, *23*–*26*), trends and constraints from evolutionary history (*27*), genetics, transcriptomics, proteomics, and isotope geochemistry (*9*) all point toward a simple but powerful plausible conceptual model for $CaCO_3$ biomineralization.

HOW DO CALCIUM CARBONATE BIOMINERALS FORM?

Carbonate biominerals grow from a chemically complex aqueous solution termed calcifying fluid (CF; see Table 1 for this and all other acronyms used throughout the text) in a biologically controlled privileged space that is bounded by a phospholipid membrane within cells and by epithelial cells in multicellular organisms. Biological processes modify the chemistry of the CF, including pH and the concentrations of calcium and carbonate ions, to increase the thermodynamic driving force for precipitation of $CaCO_3$, quantified by the saturation state of the solution, Ω, relative to the final mineral phase. Since the Ca concentration of seawater is ~10 mM and CO_3^{2-} concentration is ~0.1 to 0.3 mM, calcifiers need to concentrate

[1]Departments of Physics, Chemistry, Geoscience, and Materials Science, University of Wisconsin-Madison, Madison, WI 53706, USA. [2]Chemical Sciences Division, Lawrence Berkeley National Laboratory, Berkeley, CA 94720, USA. [3]Department of Earth, Atmospheric and Planetary Sciences, Massachusetts Institute of Technology, Cambridge, MA 02139, USA. [4]Centre Scientifique de Monaco, Department of Marine Biology, 98000 Monaco, Principality of Monaco. [5]University of Haifa, Marine Biology Department, Mt. Carmel, Haifa 31905, Israel. [6]Université de Bourgogne–Franche-Comté (UBFC), Laboratoire Biogéosciences, UMR CNRS 6282, Bâtiment des Sciences Gabriel, 21000 Dijon, France. [7]Geological and Planetary Sciences, California Institute of Technology, MS 100-23, Pasadena, CA 91125, USA. [8]The Hebrew University of Jerusalem, Institute of Earth Sciences, Jerusalem 91904, Israel. [9]Energy Geoscience Division, Lawrence Berkeley National Laboratory, Berkeley, CA 94720, USA. [10]Department of Earth and Planetary Science, University of California, Berkeley, Berkeley, CA 94720, USA. [11]Department of Organismic and Evolutionary Biology, Harvard University, Cambridge, MA 02138, USA. [12]Goethe-Universität Frankfurt, 60438 Frankfurt am Main, Germany. *Corresponding author. Email: pupa@physics.wisc.edu (P.U.P.A.G.); aknoll@oeb.harvard.edu (A.H.K.)
†Previously publishing as Gelsomina De Stasio.

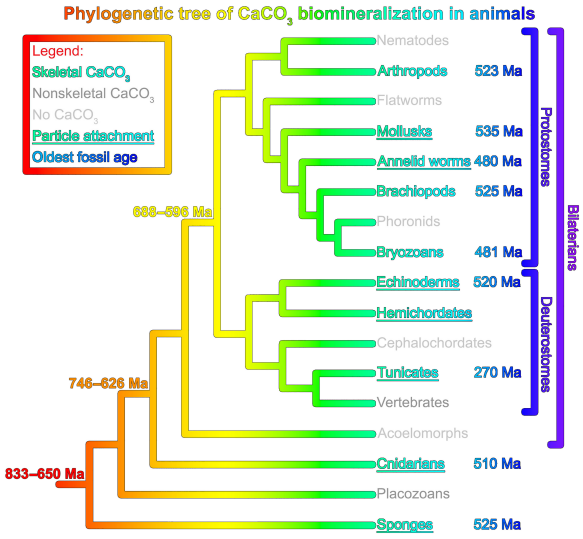

Fig. 1. Phylogenetic distribution of $CaCO_3$ biomineralization in animals. Besides animals (shown), there are species (not shown) that make $CaCO_3$ skeletons in the foraminiferans, coccolithophorids, green algae, red algae, dinoflagellates, and even a few amoebozoans and brown algae. $CaCO_3$ skeleton–forming animals are shown in turquoise font; dark gray font indicates clades that form nonskeletal $CaCO_3$ biominerals, and light gray font indicates those that do not form $CaCO_3$ at all. Skeletons confirmed to be formed in part by particle attachment (PA) are underlined, and the age of the oldest unambiguous fossil found to date is in blue font. All fossil age estimates have an uncertainty of a few million years. For hemichordates, biomineralized fossils have not yet been identified. Data are from (*15*, *215*, *242*–*246*). All clades started biomineralizing after they diverged from one another.

dissolved inorganic carbon (DIC) and elevate the pH to achieve higher CO_3^{2-} concentration and therefore higher Ω values. The organism also regulates the concentration and speciation of inorganic ions, polysaccharides, and proteins, all of which can select the mineral polymorph in the final biomineral (calcite, aragonite, or vaterite) and can vary activation barriers (and hence rates) for particle formation, phase transitions, and growth.

Nanoparticles of amorphous calcium carbonate (ACC) are a precursor phase for $CaCO_3$ biominerals formed by diverse organisms (*15*), including species from clades that diverged long before evolving calcification (Fig. 2). Abiotic studies have shown ACC precursors to be a common intermediate in the nucleation of $CaCO_3$ minerals in solution and on surfaces because this phase nucleates preferentially at a lower Ω value compared to crystalline polymorphs (*26*). Although the molecular pathways for the formation of a final crystalline carbonate via ACC are not fully established, calorimetry studies have clarified that the pathway is thermodynamically downhill (*28*). Crystalline vaterite is another transient phase, thus far observed only during test formation in foraminiferans (*29*). Following the formation of a solid-phase carbonate mineral (whether amorphous or crystalline), growth by ion attachment (IA) has far smaller activation barriers than further nucleation. These observations in natural biominerals and synthetic systems suggest that $CaCO_3$ biominerals form through a combination of ACC particle attachment (PA) and IA processes at the growth surface.

Extracellular and intracellular privileged spaces

All marine biominerals are formed within a biologically controlled compartment first termed "privileged space" in studies of sea urchin embryos (*30*). In multicellular organisms, the privileged space in which the final biomineral (e.g., skeleton) grows is bounded by a monolayer of specialized epithelial cells and contains extracellular CF (ECF). In corals, the ECF, also known as extracellular calcifying medium (ECM), lies between the calcifying cells and the growing

Table 1. Acronyms used throughout the text.

$CaCO_3$	Calcium carbonate, which comprises any of the anhydrous polymorphs of $CaCO_3$: calcite, aragonite, or vaterite
PA	Particle attachment
IA	Ion attachment
CF	Calcifying fluid
ICF	Intracellular calcifying fluid. Its existence is deduced but not yet observed.
ECF	Extracellular calcifying fluid, well documented in a variety of organisms
ECM	Extracellular calcifying medium. The ECF is termed ECM by other authors. The two are identical and interchangeable. We chose ECF because "fluid" includes liquid, dense liquid, and flowing gel phases. ECF cannot be confused with extracellular matrix, often termed ECM.
DIC	Dissolved inorganic carbon
Ω	Saturation state of a solution. Minerals precipitate and grow in supersaturated solutions (Ω > 1).
ACC	Amorphous calcium carbonate
ACC-H_2O	Amorphous calcium carbonate, hydrated
CCC	Crystalline calcium carbonate, which could be any of the anhydrous polymorphs of $CaCO_3$, calcite, aragonite, or vaterite, since all three exist as final biominerals.
CO_2	Carbon dioxide
HCO_3^-	Bicarbonate ion
CO_2(aq)	Aqueous, dissolved carbon dioxide
CA	Carbonic anhydrase, an enzyme that rapidly catalyzes the conversion of CO_2 to bicarbonate ions (HCO_3^-). CA is a membrane protein, which can also occur intra- and extracellularly and thus can be in the cytosol and presumably in the ECF and ICF. CA or CA-like proteins were shown to be an integral part of the skeletal matrix.
CoCs	Centers of calcification in coral skeletons; these are the regions of the skeleton from which all acicular crystalline fibers radiate to form plumose spherulites and are most obviously nanoparticulate.
GRNs	Gene regulatory networks
Δ[Ca], ΔpH, ΔDIC, and $\Delta\Omega_{CaCO3}$	Difference observed when comparing the CF with seawater, in calcium concentration, pH, DIC, and supersaturation with respect to relevant $CaCO_3$ mineral
EGF	Epidermal growth factor
VEGF	Vascular endothelial growth factor
LCDs	Low-complexity domains (also called compositionally biased regions) observed in proteins and characterized by the dominance of one or two amino acids. In addition, several LCDs may exhibit tandem repeats.

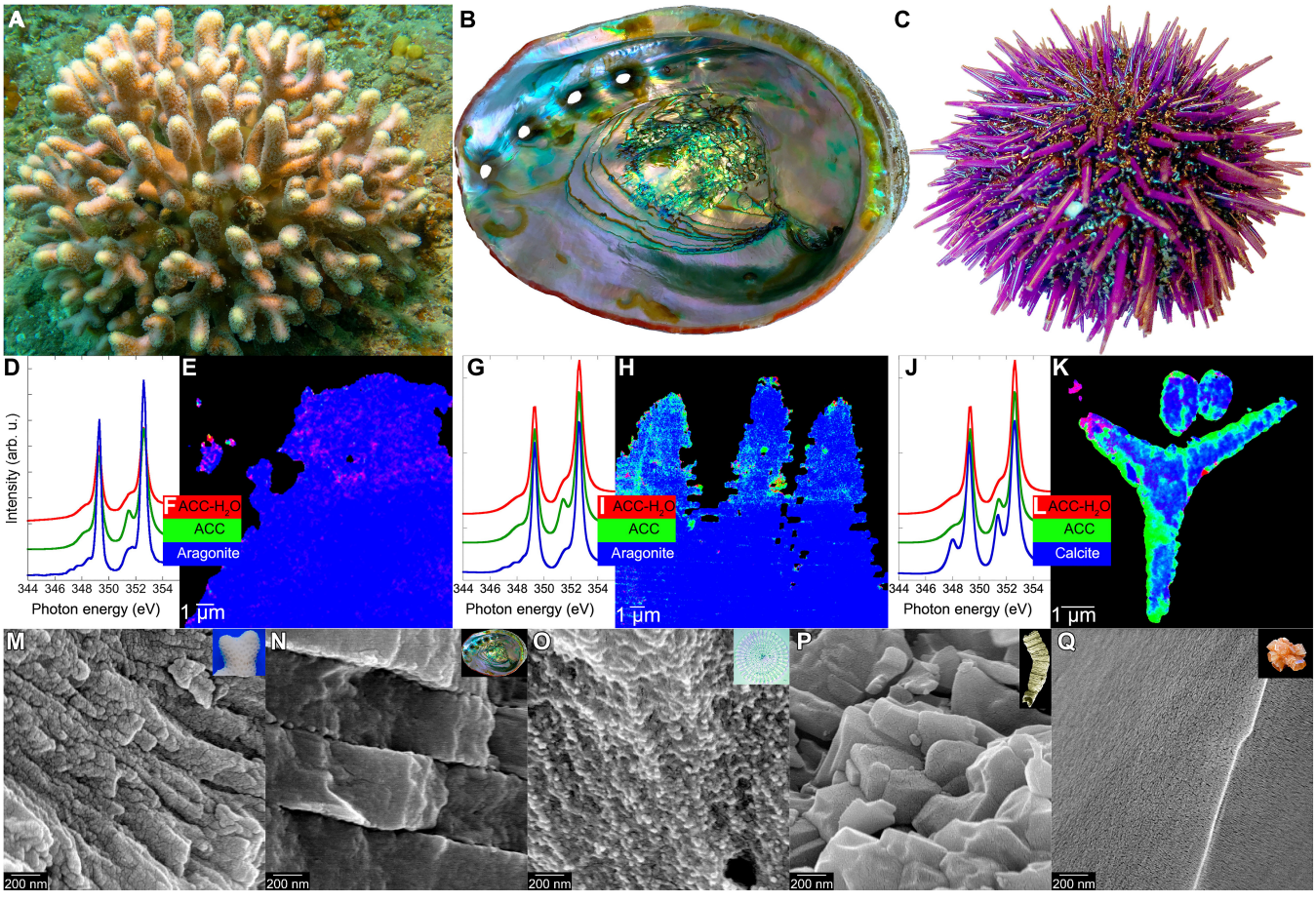

Fig. 2. The same amorphous precursors across phyla: Cnidarians, mollusks, and echinoderms. (**A**) *S. pistillata* coral in the Red Sea (photo credit: T.M.). (**B**) California red abalone *Haliotis rufescens* (photo credit: P.U.P.A.G.). (**C**) California purple sea urchin *Strongylocentrotus purpuratus* (photo credit: P.U.P.A.G.). (**D**, **G**, and **J**) X-ray absorption spectra from nanoscale regions of fresh forming biominerals: *S. pistillata* skeleton, *H. rufescens* nacre, and *S. purpuratus* embryonic spicules. Three distinct spectral line shapes at the Ca L-edge, and thus, three distinct mineral phases or "components" occur in each biomineral: hydrated ACC, anhydrous ACC, and crystalline calcite or aragonite. (**E**, **H**, and **K**) Component maps showing abundant amorphous pixels in the forming parts of each biomineral and submicrometer amorphous particles in nearby cells. (**F**, **I**, and **L**) Color legend for both component spectra (D, G, and J) and component maps (E, H, and K). (**M** to **P**) Scanning electron micrographs showing that modern and fossil biominerals show nanoparticulate texture after cryofracturing (M to P), whereas nonbiogenic minerals do not (Q). Insets in (M) to (Q) show photographs of each sample. (M and N) Modern aragonite biominerals: coral skeleton from *S. pistillata* (M) and nacre from *H. rufescens* (N). (O) Calcite sea urchin spine from *S. purpuratus*. (P) Phosphatized Ediacaran *Cloudina* (550 Ma before present) from Lijiagou, China. (**Q**) Nonbiogenic aragonite from Sefrou, Morocco. Data are from (*15*, *23*–*25*). arb. u., arbitrary units.

skeleton (*31*); in mollusks, the ECF is the extrapallial fluid in a compartment between the mantle and the growing shell (*32*); in sea urchin embryos, the ECF is a spicule-shaped compartment termed syncytial envelope in which a calcite spicule grows (*33*, *34*). In foraminiferans, which are single-celled amoeboid protists, the test forms from the ECF within a specialized membrane-bound compartment, formed by endocytosis of seawater (*35*, *36*). Coccolithophorids, single-celled algae that are major contributors of calcium carbonate to the deep seafloor, also have specialized membrane-bound compartments, likely derived from preexisting organelles such as the Golgi apparatus (*18*), that provide the privileged space in which each mineralized coccolith grows (*37*, *38*).

It is well established that intracellular vesicles play key roles in concentrating the ions required for biomineralization, in transporting them to the ECF, and likely in mineral deposition. The existence of intracellular reservoirs of DIC used for skeleton deposition, termed "DIC pool," was first proposed on the basis of the comparison of ^{14}C and ^{45}Ca uptake kinetics (*35*, *39*–*42*). Subsequent imaging and microchemical studies have revealed the intracellular vesicles and vacuoles providing DIC pools in numerous organisms. For example, in foraminifera, vacuoles contain chemically modified seawater (*35*, *36*), as well as smaller Mg- and Ca-rich vesicles (*43*). Elevated Ca in intracellular vesicles is observed in coral cells (*44*), sea urchin embryos (*45*–*47*) and spines (*48*), and coccolithophorids (*49*).

Vesicles can also be locations where initial biomineral-forming ACC nanoparticles are nucleated, as first hypothesized by Cohen and McConnaughey (*50*) for the case of coral skeleton formation. Now, evidence for such intracellular precursor nanoparticles is overwhelming in the tissue adjacent to the forming surface of coral skeletons (*25*, *51*–*53*), in sea urchin embryonic cells forming spicules (*47*), and in the tissue regenerating adult sea urchin spines (*48*). Cells extracted from coral polyps cannot form a tissue-bounded privileged space with an ECF, yet they are able to form carbonate crystals, likely explained by calcification in intracellular vesicles (*54*). Thus, some,

possibly all, biomineralizing organisms use vesicles containing intracellular CF (ICF) to initiate $CaCO_3$ precipitation.

Privileged space chemistry is under biological control

Marine biominerals form from seawater, but they do not form in seawater. The composition of the CF in the privileged space (ICF and ECF) is seawater modified chemically and isotopically by active biological control. Microelectrode studies of corals (*31*, *55*, *56*) have provided the most compelling and direct characterization of the chemical conditions of the privileged space. Sevilgen *et al.* (*31*) demonstrated that pH and CO_3^{2-} and Ca concentrations in the ECF of *Stylophora pistillata* corals are all elevated relative to surrounding water, enabling the saturation state with respect to aragonite ($\Omega_{aragonite}$ ~12) to be calculated. Further evidence for biological control comes from measurements of boron isotopes in $CaCO_3$ that are sensitive to the fluid pH during carbonate formation. Tropical, temperate, and cold-water coral species maintain an approximately constant pH difference between seawater and ECF (*57*, *58*). The capability of maintaining elevated pH in the CF at the sites of calcification in artificially acidified waters was recently demonstrated across a range of phyla (*59*). Studies of single-celled organisms are more challenging, but Taylor *et al.* (*18*) used electrophysiological and genetic approaches to demonstrate that coccolithophorids elevate coccolith vesicle pH using voltage-gated membrane H^+ channels. Ter Kuile *et al.* (*39*, *40*) and Bentov *et al.* (*35*) showed that foraminifera ECF has greater DIC and pH with respect to seawater. Higher DIC and pH produce higher supersaturation with respect to calcite $\Omega_{calcite} \approx 30$ to 40 in foraminifera ECF. Kahil *et al.* (*47*) isolated spicule-forming single cells from sea urchin embryos and demonstrated that each cell contains hundreds of intracellular vesicles and that the ICF in these vesicles is much richer in Ca compared to seawater.

Privileged spaces are never completely isolated from seawater

Marine biomineralizers may use a combination of active and passive mechanisms, transcellular and paracellular pathways, to control the chemistry of the privileged space. Active mechanisms include solute passage through transmembrane transporters and fluid transport by pinocytosis, as observed in foraminiferans (*35*, *36*) and corals (*60*). Passive mechanisms include water passage through aquaporins, CO_2 diffusion through membranes, and paracellular transport between cells. Regardless of the mechanism, the maintenance of a thermodynamic gradient between seawater and the privileged spaces requires the expenditure of energy by cells. A notable example of privileged space partly open to seawater was found in coral, where junctions between epithelial cells enable passive diffusion of ions and molecules selected by charge and size but always smaller than approximately 20 nm in adult corals (*61*) or larger in primary coral polyps (*52*). The degree to which the privileged space is open to the environment affects the control of chemistry (*62*) and likely affects the susceptibility of marine biomineralizers to changes in seawater conditions.

$CaCO_3$ biomineral growth by amorphous particle and ion attachment

Many previous models for biomineral formation described two contrasting mechanisms: IA from a CF (*63*–*65*) or PA of ACC precursors from intracellular vesicles (*15*, *25*, *26*, *45*, *47*, *48*, *53*, *66*). IA is unavoidable in the presence of a CF that is rich in ions and supersaturated with respect to the final biomineral (*31*, *64*, *67*, *68*), yet evidence for PA of ACC precursors is abundant (*15*, *25*, *26*, *45*, *47*, *48*, *53*, *66*, *69*). Here, we propose a mechanistic model that includes both PA and IA.

ACC precursors to $CaCO_3$ biominerals

In 1997, Beniash *et al.* (*70*) demonstrated that embryonic sea urchin spicules form via an ACC precursor. Later, ACC was identified by Weiss *et al.* (*71*) in mollusk embryonic shells and by Politi *et al.* (*72*) in regenerating sea urchin spines. In 2008, Politi *et al.* (*73*) demonstrated using synchrotron spectromicroscopy that, at the nanoscale, there are two amorphous precursors to crystalline calcite in sea urchin spicules, hydrated (ACC-H_2O) and anhydrous ACC. The same two ACC precursor phases were then detected during the formation of sea urchin teeth (*74*); in sea urchin spicules, again, to indicate the sequence of phases and phase transitions (*24*); in mollusk shell nacre (*23*); in corals skeletons from *S. pistillata* (*25*); and from five additional reef-forming coral species (*51*).

The unexpected discovery of the same precursor phases to aragonite and calcite biominerals, in phyla drawn from three major branches of eumetazoan phylogeny (cnidarians, mollusks, echinoderms) (*8*), which diverged from one another long before they started making biominerals (Fig. 1) (*15*), suggests that this biomineralization strategy emerged independently in these distantly related clades. Because skeletons formed in this way preserve a nanoscale textural record of the ACC PA by which the skeletons formed, Gilbert *et al.* (*15*) were able to show that this mineralization pathway was already used by Cambrian mollusks (~500 Ma before present) and even by the iconic Ediacaran fossil *Cloudina*, one of the first animals to form a $CaCO_3$ skeleton, some 550 million years ago. These results are summarized in Fig. 2.

PA + IA growth is rapid, space-filling, and makes tougher biominerals

Crystal growth by PA is much faster than by IA. A notable example is provided by eggshells, which grow faster than any other known biomineral: Hen eggshells grow to 300 μm in thickness in 24 hours, with PA of 100- to 300-nm ACC particles that subsequently crystallize to calcite (*75*). Ostrich eggshells grow to 2 mm in thickness in 48 hours (*76*), making them the fastest-growing of all biominerals. Coral skeletons of *S. pistillata* grow, on average, ~40 μm/day (*77*–*79*) by PA of 100- to 400-nm ACC particles, which then crystallize to aragonite (*25*). By contrast, the rate of abiotic aragonite growth by IA from seawater is on the order of 0.01 to 0.1 μm/day (*80*–*83*). Five other reef-forming coral species were recently demonstrated to form skeletons and fill space by PA + IA (*51*). The impact of PA is perhaps best illustrated by the Great Barrier Reef, the largest of all biomineral structures, which is visible from outer space, and stretches continuously for 2300 km from north to south along the coast of Queensland, Australia.

Identical particles at any scale, from the nano- to the macroscale, can never fill three-dimensional space (*84*), not even in the most space-filling hexagonal close packing. This is the configuration of identical cannonballs stacked on one another in three-dimensional arrays: A considerable amount of space, 26%, remains unfilled as cannonballs fill 74% of space. Particles of different sizes can fill >74% of space but never 100% (*84*). However, surface area data show that sea urchin spines and coral skeletons are 100% space-filling as are abiotic single crystals of calcite or aragonite, respectively (*51*, *85*, *86*). In the PA + IA model, PA fills part of the space, and ions fill the remaining interparticle voids as recently concluded by Walker *et al.* (*37*) for coccolithophorids and by Sun *et al.* (*51*) for coral skeletons.

The mechanical properties of biominerals are greatly improved by PA, even when the final biomineral is single crystalline, and the originally ACC nanoparticles crystallize to become coherently aligned

(*87*). Crystalline defects accumulating at nanoparticle interfaces deflect and dissipate cracks and therefore toughen the biomineral (*87*–*89*).

Morphogenesis by PA + IA of mesostructured biominerals

Despite the apparent universality of the PA + IA pathway, the carbonate minerals in skeletons vary widely in form, orientation, size, and mineralogy, sometimes within a single individual. Termed mesostructure, the size, shape, crystal orientation, and spatial arrangement of crystals underpin biomineral function. The controlled crystal growth manifest in mesostructural diversity is mediated by an array of structural proteins, including enzymes, glycoproteins, and polysaccharides, all of which are present in the privileged space, are incorporated in the biomineral, and are therefore termed "organic matrix." De Yoreo and Dove (*90*) showed that growing crystals can be shaped by organic molecules, and other experiments have demonstrated polymorph selection by the entire organic matrix mixture of organic molecules (*91*, *92*), by single proteins (*93*–*96*), or by short peptides (*97*). The latter not only served as templates for the formation of aragonite under calcite growth conditions (no Mg) but also self-assembled into organic layers that alternated with lamellar aragonite, similar to nacre (*97*). Recent work by Mummadisetti *et al.* (*98*) documented the function and fine-scale spatial organization of these matrix molecules in stony corals.

The organic matrix, presumably, must also control the cessation of crystal growth, that is, inhibit or poison it, as proposed by Addadi and Weiner (*99*). In this regard, Yang *et al.* (*100*) recently demonstrated that a previously unidentified matrix protein called PfX binds to specific crystal faces in developing shells of *Pinctada fucata*, thus helping to shape carbonate crystal growth. Inhibiting nucleation and growth of crystals at the wrong place and time is also a key role for organics (*99*, *101*). How organics control crystal orientation tilting, however, is not understood (*102*–*104*) nor is the role of organics-associated cations in crystal orientation control (*105*).

An integrated model for $CaCO_3$ biomineralization

A mechanistic model for marine $CaCO_3$ biomineralization is presented in Fig. 3. The model builds upon prior proposals for individual species or phyla [e.g., corals (*50*, *106*–*108*), coccolithophorids (*18*, *109*), and foraminiferans (*35*, *110*)] but hypothesizes that the fundamental geochemistry of carbonate species and minerals plus the functionally equivalent strategies for transport and mineral formation result in an evolutionarily convergent shared framework despite the diversity of marine biomineralizing organisms. In particular, the model hypothesizes that amorphous particle formation in vesicle ICF and biomineral growth by IA in the ECF, along with PA, is a general strategy. Amorphous precursors or PA have not been observed in brachiopods or foraminiferans; they are simply hypothesized here. We propose that variation in the contributions and rates of the mechanisms in Fig. 3 could explain observed differences in carbonate biomineral isotopic and elemental composition. Although more work is needed to quantify these contributions, and to incorporate photosynthesis, this model provides the framework for understanding the ability of marine calcifiers to act as paleoenvironmental proxies, their vulnerability or resilience to stressors associated with past or present climate change, and the commonality of nanostructures observed in the fossil record across phyla (*15*). For example, in corals, the pH, calcium, and carbonate ion concentrations in the ECF are greater than those in seawater (*31*, *67*, *111*, *112*), as indicated by the magenta deltas in Fig. 3. A similar observation is expected in other organisms as well (*113*). Whether these are constant offsets, varying as the seawater values vary (*112*, *114*, *115*), or are maintained constant at homeostatic values (*116*, *117*) may affect the energy cost of calcification.

The extent of PA versus IA varies across organisms. Extremes are coccolithophorids, skewed toward IA (*37*, *38*, *49*), and sea urchin spicules, preferentially growing by PA (*24*, *26*).

To test or falsify the model, two principal directions are possible. One is to explore whether carbonate biomineralization involves a sequence of thermodynamically downhill carbonate phases in many more organisms. Recent observations of a transient liquid precursor to sea urchin spine formation, or a transient vaterite phase during test biomineralization by foraminiferans (*29*), are consistent with the model but require a richer number of phases and phase transitions currently not included. Another option is to establish compositional relationships between seawater, CF, precursor particles, and the final skeleton, consistent across organisms, natural biominerals, and reproducible in laboratory experiments. For example, if future synthetic experiments find that formation via amorphous (*51*) or crystalline (*29*) precursors markedly affects isotopes in the laboratory, but biominerals are isotopically more similar to seawater than to synthetic precursors, then the model with PA + IA must be reconsidered.

A weakness of the model is that ICF is only reasonably deduced to exist in most organisms; it has only been observed and measured directly during the formation of sea urchin spicules (*47*) and indirectly during sea urchin spine (*48*) and coral skeleton (*53*) formation. Thus far, the best characterized CF is the ECF in one coral species, *S. pistillata* (*31*, *67*, *111*, *112*). Only carbonate chemistry was measured in *S. pistillata*, whereas the pH was measured in the ECF of more coral species and found to differ significantly between day and night (*53*, *112*), highlighting the other weakness of the model: the lack of photosynthesis and related pathways.

As the model in Fig. 3 shows, biomineral formation takes place in a privileged space, which may be intra- or extracellular and is separated from but partly open to seawater, and its chemical composition is biologically controlled. All organisms actively concentrate Ca and DIC into ICF and ECF and actively remove protons from both. Passive diffusion of carbon dioxide [CO_2(aq)] occurs through all cell and vesicle membranes. At the same time, mitochondria respire and produce CO_2, which in part diffuses toward seawater, ECF, and ICF and in part is rapidly converted to bicarbonate ions (HCO_3^-), as catalyzed by carbonic anhydrase (CA) in the cytosol and in ICF and ECF. This additional bicarbonate is also pumped actively into ICF and ECF, where, at higher pH, its speciation changes to carbonate ions CO_3^{2-} that readily bind Ca^{2+}. Besides calcium and carbonate, organic molecules synthesized by the organism are also injected into the vesicles and the ECF and form the organic matrix occluded in the biomineral.

ISOTOPE AND TRACE ELEMENT SUPPORT FOR AN INTEGRATED MODEL OF BIOMINERALIZATION

Marine calcifiers incorporate elements and isotopes into their biominerals at levels that are partly determined by seawater concentrations, providing the basis for paleoenvironmental proxies, and partly determined by the biological and geochemical processes that modify the chemistry and isotopic composition of the ICF and ECF. As a consequence of such processes, termed "vital effects," biomineral compositions may depart from those observed in abiotically precipitated minerals under the same seawater conditions. These vital effects not

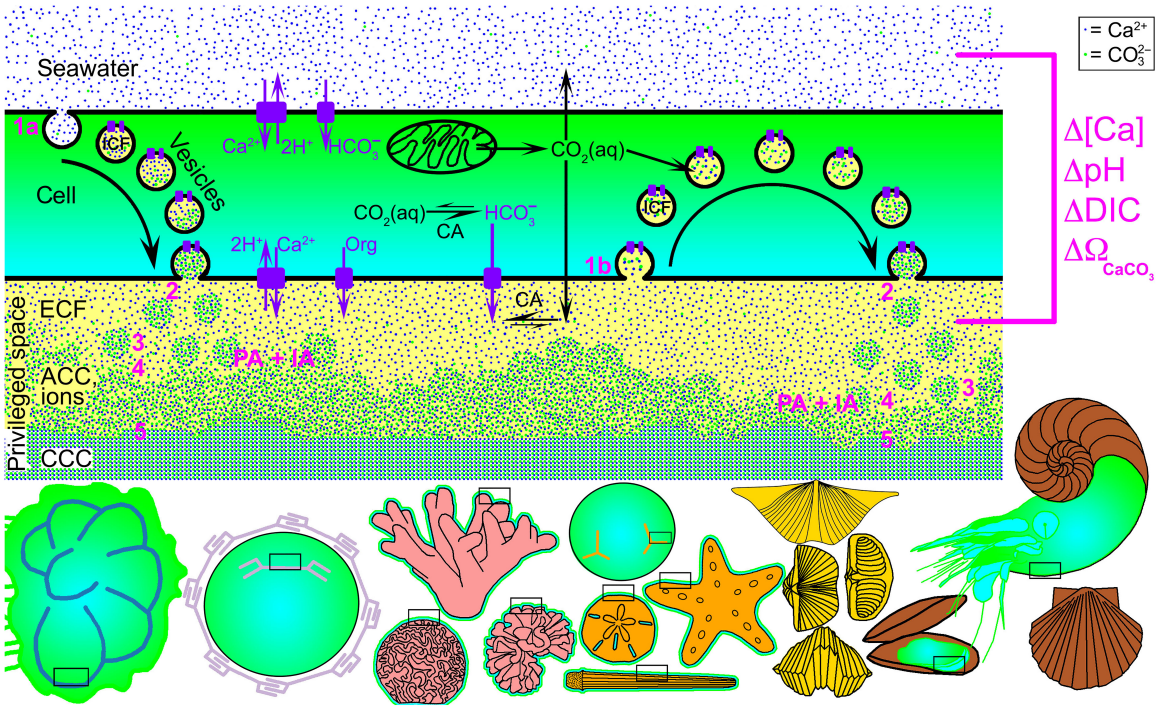

Fig. 3. Integrated model for $CaCO_3$ biomineralization mechanisms in all marine organisms. Biomineralization takes place in a privileged space, shaped for the biomineral function, which may be intra- or extracellular, is separated from but partly open to seawater, and is chemically different from seawater (magenta deltas, right). The cell (green and cyan) can be a single cell (e.g., in foraminiferans or coccolithophorids) or part of a layer of cells (e.g., mantle epithelial cells in mollusks), or there may be additional tissue layers (e.g., in sea urchin embryos, spines, teeth, or coral polyps). The privileged space contains an intra- or extracellular calcifying fluid (ECF or ICF; yellow) modified with respect to seawater (*31*). All acronyms in the model are defined in Table 1. ICF is either endocytosed seawater (step **1a**), as observed in foraminiferans but not in corals (*61*, *247*), or ICF is endocytosed ECF (step **1b**), as observed in corals (*60*). In either case, the ICF is actively enriched in Ca and CO_3 ions by membrane transporters across all cell and vesicle membranes (purple rectangles), and protons are removed to increase pH and form ACC. In step (**2**), ACC-H_2O solid particles are exocytosed into the ECF. In (**3**) and (**4**), particles and ions attach to the biomineral growth front and remain ACC for up to 45 hours (*23*–*25*, *53*). In the last step (**5**), particles and ions crystallize into crystalline calcium carbonate (CCC; either calcite, aragonite, or vaterite). Both particle and ion attachment (PA + IA) occur at the biomineral growth front. At the bottom, schematic representations of a foraminiferan, a coccolithophorid, three corals, four echinoderms, four brachiopods, and three mollusks show biominerals (colored as in Fig. 4). In all organisms, cells are shown in green and cyan, and black boxes indicate the region where the above model actively deposits biomineral.

only can hinder the reconstruction of paleoenvironmental conditions using fossils (*41*, *57*, *65*, *107*, *109*, *118*–*126*) but can also test the $CaCO_3$ biomineralization model because isotopic and trace element concentrations are affected by factors such as ion sources, rates of transport, CA activity, and ICF or ECF fluid conditions. Although the relevant studies have not yet been performed, trace element and isotope signatures may also be affected by the relative contributions of PA and IA. In different phyla, variations in the competing rates and pathways of calcification, element exchange, and isotope fractionation can lead to different expressions of the vital effects within the same plausible model.

Understanding the isotope and trace element compositions of $CaCO_3$ biominerals can also provide insight into the susceptibility of skeleton formation to ocean acidification. Trace element or isotope incorporation into biominerals cannot be understood quantitatively without making assumptions about whether the trace species fully, partly, or negligibly equilibrate with a large reservoir as the skeleton is deposited. Attaining consistent understanding of the open/closed system behavior from both trace elements and isotopes in biominerals could constrain estimates of the fluid and element fluxes required for calcification and thus determine the openness of the ECF and ICF to seawater protons.

Boron and its isotopes

Boron and $\delta^{11}B$ in coral skeletons can be used to reconstruct the pH and carbonate chemistry of the ICF and ECF (*127*–*129*). Specifically, with key assumptions, $\delta^{11}B$ provides the pH and the B/Ca ratio provides $[CO_3^{2-}]$ in the ECF. In coral, boron estimates of CO_3^{2-} and $\Omega_{aragonite}$ are in excellent agreement with direct observations of the ECF obtained using microelectrodes and fluorescent dyes (*31*, *67*, *111*, *112*). The $\delta^{11}B$ measured in $CaCO_3$ biominerals from diverse taxa demonstrates the ability of many organisms to elevate pH in the ECF or ICF relative to seawater (*59*). Elevated pH values inferred from $\delta^{11}B$ measurements (Fig. 4, A and B) agree with other techniques that measure elevated pH within the ECF and ICF. Some of the highest pH values are often observed using fluorescent dyes at the onset of calcification or in vesicles (*130*–*132*), consistent with ACC formation in intracellular vesicle ICF.

The pH inferred from $\delta^{11}B$ measurements in Fig. 4 (A and B) shows that, except for deep-sea corals, the other heterotrophs analyzed form their biominerals in ICF and ECF with pH similar to seawater pH, whereas photosynthetic organisms or heterotrophs with symbionts have more scattered and more elevated pH estimates from $\delta^{11}B$ relative to seawater pH. Thus, photosynthesis is one process that makes it easier to increase pH in the ICF and

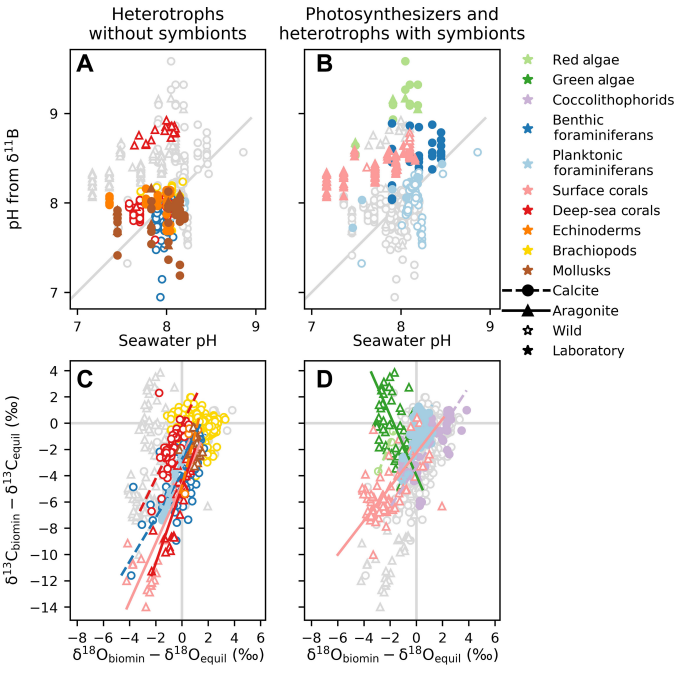

Fig. 4. Meta-analysis of the boron, carbon, and oxygen isotopic ratios observed in a variety of taxa. Each taxon is colored as the corresponding biomineral in the drawings of Fig. 3. (**A** and **B**) Inferred pH from $\delta^{11}B$ measured in biominerals versus seawater pH, using expected thermodynamic equilibrium for the borate ion at in situ temperature, salinity, and depth (*248*). The 1:1 line is shown in gray. (**C** and **D**) $\delta^{13}C$ versus $\delta^{18}O$ normalized to the expected values for inorganic calcite or aragonite in equilibrium with the relevant environment. In all panels, data are plotted separately for heterotrophs without symbionts (A and C) and for photosynthesizers and heterotrophs with photosynthesizing symbionts (B and D). In all plots, the data from the other group are displayed in light gray for reference. As indicated by the black symbols in the legend, circles or triangles represent calcite or aragonite, respectively; empty or filled symbols correspond to wild or laboratory-reared organisms. Linear fits to C and O data for each taxon data are plotted with the same taxon color, with dashed or solid lines for calcite or aragonite, respectively (C and D). Brachiopods and mollusks do not show a linear trend. All data in the meta-analysis (~2500 data points) and all the references from which the data were collected are available for download from (*241*), along with a preprint of this figure, many ancillary figures, and the code for analyzing and plotting them.

ECF. This is not unexpected, as symbiotic algae are known to influence intracellular pH in corals by taking up CO_2 for photosynthesis (*112*). Laurent *et al.* (*133*) showed that intracellular pH can rise significantly during the day and return to equilibrium with seawater at night, consistent with greater daily calcification of coral skeletons. In some corals (e.g., *Acropora hyacinthus*), during acidification experiments, part of the skeleton even dissolves at night but grows during the day, as ECF pH drops at night (*53*, *112*). Thus, ICF and ECF pH fluctuates with photosynthesis. Multiple species of heterotrophic, aragonitic deep-sea corals also have elevated pH estimates from $\delta^{11}B$ (Fig. 4A), suggesting that they expend considerable energy to increase pH in their ICF and ECF to values similar to surface corals, perhaps to combat acidic deeper water environments (*58*, *134*, *135*).

Linear trends in biomineral carbon and oxygen isotopes

We conducted a meta-analysis of the previous literature on the carbon and oxygen isotopic composition of $CaCO_3$ skeletons to investigate the degree to which these isotopes covary across marine calcifiers, as first described by Keith and Weber (*11*) and by McConnaughey (*136*). Plotting $\delta^{13}C$ versus $\delta^{18}O$ shows that environmental variability contributes considerably to the spread of both variables (*50*). Thus, we sought to isolate vital effects by removing the expected contributions of varying mineralogy, DIC $\delta^{13}C$, temperature, and water $\delta^{18}O$. These results also highlight critical differences between biomineralization in heterotrophs and photosynthetic organisms or organisms that host photosymbionts. These groups are separated and presented in Fig. 4 (C and D). For each measurement, we plotted the difference between biomineral $\delta^{13}C$ and $\delta^{18}O$ and estimated mineral-specific $\delta^{13}C$ and $\delta^{18}O$ for inorganic carbonate precipitated in equilibrium with local seawater. If a given biomineral had no vital effect or offset from the inorganic expectation from seawater $\delta^{18}O$ and DIC, then it would plot at 0,0 (gray lines). Note that some residual environmental effects unavoidably remain, as some environments see substantial seasonal DIC $\delta^{13}C$, T, or water $\delta^{18}O$ variability. For all biominerals that depart from expected equilibrium, the anomaly in $\delta^{13}C$ is greater than that in $\delta^{18}O$.

The data show that multiple heterotrophic taxa display a tendency to form carbonates that are more depleted (that is, they have lighter isotopes) in ^{13}C and ^{18}O than expected for carbonates formed at equilibrium with the surrounding seawater (*118*). The $\delta^{13}C$ and $\delta^{18}O$ data strongly covary and show linear trends (see linear fits in Fig. 4C), implying a commonality of process across taxa. Results that covary represent variability both within individuals (i.e., corals and echinoderms) and across individuals including from experiments that sample different conditions (e.g., foraminifera grown at different pH). Notably, isotopic data from brachiopods and mollusks are the exception and do not display a linear trend in $\delta^{13}C$ and $\delta^{18}O$. In estuarine bivalve shells, this may be explained by the extreme variability of coastal water salinity, which markedly affects both $\delta^{18}O$ and $\delta^{13}C$ (*137*, *138*) and is not subtracted in Fig. 4.

Taxa with photosymbionts (i.e., surface corals and planktonic foraminifera) can also display covariance, but the slopes are shallower (Fig. 4D). Photosynthetic organisms, as individuals or as symbionts, also create light organic carbon from DIC during photosynthesis. This process, and how carbon pools are distributed across taxa, can reduce the magnitude of depleted carbon isotopic compositions recorded in surface corals or even create a positive enrichment in $\delta^{13}C$ biomineral relative to DIC (i.e., green algae). Planktonic foraminifera with symbionts are most likely to be near 0,0 in Fig. 4D. Important common aspects are known and understood, represented in the model of Fig. 3, and discussed hereafter.

There are two sources for the ^{13}C-depleted intracellular C incorporated into biominerals: CO_2(aq) within DIC that is 9 to 12 per mil (‰) lighter than HCO_3^- and CO_3^{2-} in seawater and metabolic CO_2 resulting from the respiration of organic molecules (*139*), which can be more than 20% of the C in some biominerals (*42*, *140*–*142*). CO_2(aq) from both sources, DIC and metabolic, is the sole DIC species that can readily diffuse across cell and vesicle membranes because it is a small, neutral molecule (*107*, *118*, *136*). ^{13}C-depleted CO_2(aq) is, therefore, an important and abundant source of carbon for the ICF and ECF, at the high pH of the CF (*118*). Diffusing ^{13}C-depleted CO_2(aq) mixes with more ^{13}C-enriched HCO_3^- transported by transmembrane anion transporters (*143*–*146*) and with seawater actively transported by vesicles or by passive paracellular transport into the ICF or in the ECF where IA and PA occur.

Departures from expected $\delta^{18}O$ and $\delta^{13}C$ equilibrium values have been suggested to include influences from the following: (i) the

massive reservoir of ^{18}O in water and the separate equilibrium fractionation factors between water and the various carbonate species (*118*, *147*–*149*), (ii) kinetic isotope effects associated with rapidly transforming CO_2(aq) from either DIC or metabolic sources via hydration and hydroxylation reactions into carbonic acid and bicarbonate (*136*, *150*, *151*), (iii) isotopic effects associated with the formation of ACC and subsequent PA (*152*), and (iv) photosynthesis. Recent modeling work suggests that the kinetic fractionation associated with the hydration reaction is likely a substantial contribution to the observed linear trends in heterotrophs in Fig. 4C (*150*, *151*). CA, which catalyzes reversibly the hydration of CO_2 and dehydration of HCO_3^- and is found in the shell-associated proteome (*153*) and localized to the CF in corals (*141*), accelerates isotopic equilibration with the CF. CA activity, in particular, has been proposed by Chen *et al.* (*107*) to modify the slope of the linear trend expected from the hydration reaction.

The roles of amorphous precursors and PA in the preserved isotopic variability are less well understood. Few studies have explored the isotopic consequence of carbonate formation via amorphous precursors [see (iii) above], but evidence from trace element studies (*154*, *155*) suggests that ACC formation may capture solution species without exchange. Thus, rapid precipitation of ACC could help preserve depleted kinetic isotopic signatures associated with the hydration or hydroxylation reactions.

In support of this model, the most depleted ^{13}C and ^{18}O data points of each taxon dataset are often generated in specific anatomical positions known to involve PA. For example, in both deep-sea and surface corals, morphological evidence suggests that PA has a more substantial role in forming centers of calcification (CoCs): The CoCs consistently exhibit the most obviously nanoparticulate crystal texture (*86*), and they are also the most isotopically depleted in both $\delta^{13}C$ and $\delta^{18}O$, compared to aragonite crystal fibers in the same coral skeletons (*118*).

We hypothesize that $\delta^{13}C$ and $\delta^{18}O$ are affected differently by PA or IA biomineral formation, but this has not been studied thus far. Particles are formed in vesicle ICF, whereas IA occurs from ECF solution, and the two liquids are most likely different in pH and carbonate saturation state, which affects the nucleation (thus PA) and growth (by IA) of crystals, as shown by Cohen and Holcomb (*156*, *157*). Sevilgen *et al.* (*31*) measured $\Omega_{arag} = 12$ in coral ECF, which is high enough for IA but not for nucleation (*157*). In vesicles, the supersaturation must be greater, $\Omega_{ACC\text{-}H_2O} \geq 20$ (*157*), to enable both nucleation and growth of ACC particles. Particles precipitating from greater supersaturation are expected to precipitate faster and thus be kinetically depleted in ^{13}C and ^{18}O. This hypothesis could be tested in future nanoparticulate cryofracture experiments in organisms that show depletion in ^{13}C and ^{18}O, similar to those in Fig. 2 (M to O).

Trace and minor elements

The incorporation of trace and minor elements and their stable isotopes into $CaCO_3$ skeletons has been studied extensively, including Li, B, Na, Mg, Sr, and Ba in coral skeletons (*115*, *120*, *158*–*163*) and Li, Na, Mg, Sr, Cl, and F in foraminiferan tests (*105*, *164*–*167*). Trace and minor element compositions of these biogenic carbonates deviate from calcite and aragonite precipitated abiotically from seawater (*161*, *164*). Such deviations were also observed in biominerals formed by mollusks and coccolithophorids (*120*, *161*, *168*–*170*). One effect of the mineralization pathway by PA + IA, as opposed to IA alone, is the increase in incorporated minor and trace elements in $CaCO_3$, as shown by in vitro experiments and in $CaCO_3$ biominerals (*115*, *155*, *171*, *172*).

Quantitative observations of trace and minor element incorporation suggest that the ECF can be a closed system. In this closed-system model, calcium concentration in the ECF is initially similar to seawater; then, as $CaCO_3$ precipitates in ICF and the biomineral grows by IA from ECF, the latter becomes depleted in Ca and slightly enriched in Mg, Na, and Li, because these elements are less incorporated into solid $CaCO_3$, compared to Ca. Other elements that are preferentially incorporated in minerals precipitated abiotically from seawater, such as Cd in calcite or Sr in aragonite, are detected at lower concentrations in biominerals; thus, the ICF or ECF from which they precipitate is inferred to be depleted in these elements compared to seawater. This is observed in foraminiferans (*168*, *173*), including comparison of Cd in symbiont-bearing and non–symbiont-bearing foraminiferans (*174*), and in corals (*65*, *161*). Such closed-system ECF behavior is consistent with the model in Fig. 3 but does not take into account the paracellular transport of seawater, which is passive diffusion between cells, and it means that the ECF is at least in part open to seawater (*62*, *68*). Because of such seawater leakage, Cd and Sr observed in biominerals with respect to abiotic precipitates can be more or less depleted than they would be in completely closed systems.

In partly closed–system ICF and ECF privileged spaces, biomineral formation by PA may be enriched in certain elements (Mg, Na, and Li) and depleted in others (Cd in calcite or Sr in aragonite) more than by IA. This is because the volume of modified seawater from which particles precipitate or IA takes place is markedly different. The vesicles contain small volumes $(\sim 100\ nm)^3$ of intracellular ICF (*15*), whereas the ECF volume is on the order of $(1–10\ \mu m)^3$. Thus, if the volume of water with which to exchange ions during formation matters, trace and minor element concentrations may be even more informative than isotopes in determining the relative amounts of PA from ICF and IA from ECF in each biomineral.

INTEGRATING MECHANISM AND EVOLUTION

Phylogeny and genomics/proteomics provide comparative biological insights into $CaCO_3$ biomineralization, and the fossil record places this portrait in historical perspective. Together, they then permit inferences about skeletal evolution. The number of independent origins of carbonate skeletons in animals has variously been estimated from as few as 8 (*156*) to as many as 40 (*175*, *176*), with intermediate numbers proposed as well (*157*); without question, animals with carbonate skeletons have evolved repeatedly from unmineralized ancestors. Despite this diversity, the shared biomineralization mechanisms, summarized in Fig. 3, suggest that the phylogenetically distinct instances of carbonate biomineralization co-opted similar basic features of cell biology.

Moreover, there is isotopic and structural evidence that some biomineralizers followed parallel evolutionary trajectories, with trends toward increasing control of the privileged space (*177*, *178*) and toward increasingly complex mesostructure (*179*, *180*). Although there is less knowledge at present about how organisms coordinate gene expression for skeletogenesis and morphogenesis, it is plausible that the diverse biomineral structures observed across phyla result from relatively small changes to the genetic recipes for how to combine the few ingredients of carbonate materials chemistry.

Co-optation and evolution of biomineralization molecules

Lowenstam and Margulis (*181*) proposed long ago that key molecular pathways used by biomineralizers must have long predated biomineralization per se and that the internal regulation of calcium ion fluxes was a prerequisite step before calcification. Genomic and transcriptomic studies provide support for this fundamental insight, with evidence that biomineralization evolved by the co-optation of proteins and other molecules that earlier served other essential biological functions.

Soon after the first sea urchin genome sequence was published (*182*), Livingston *et al.* (*183*) searched for and found biomineralization-related genes that were common to echinoderms and vertebrates, leading them to propose that a common "toolkit" of genes governs carbonate biomineralization. When Jackson *et al.* (*184*) compared nacre-associated genes between bivalves and gastropods, however, they found only 10% commonality in gene sets, despite the macro- and microscopic similarity of nacre in these two molluscan classes. Even within a single valve of the marine bivalve *Pinctada margaritifera*, Marie *et al.* (*185*) found that the prismatic and nacre layers are associated with completely different secreted proteins.

As genomic and proteomic datasets have multiplied, this pattern of both unity and diversity in molecular constituents has been reinforced: A limited set of genes and proteins are distributed widely among carbonate biomineralizing animals, whereas most genes have limited phylogenetic distribution (*99*, *186*–*189*). Genes and proteins conserved among a phylogenetically wide sampling of animals are mostly those associated with fundamental aspects of cell and tissue function, likely found in the last common ancestor of all animals. These protein domains have likely been recruited/co-opted independently in the different metazoan lineages when they started to calcify. These include CA, tyrosinase, protease inhibitors, chitin-binding proteins, and diverse proteins with an extracellular matrix signature (*107*, *187*, *189*–*193*).

As recognized explicitly by Jackson and Degnan (*194*), skeletal growth closely matches other aspects of ontogeny; thus, biomineralization must be integrated into the overall developmental program of animals. The evolution of early biomineralization likely involved the repurposing of ancestral gene regulatory networks (GRNs), that is, sets of genes that control the differential expression of themselves or other genes for development and morphogenesis. GRNs have been identified in modern sea urchins (*195*, *196*) and mollusks (*145*), where they regulate the expression of the protein transporters that control CF chemistry in privileged spaces (*145*, *146*). These proteins, therefore, are the ones that maintain the offsets observed between ECF and seawater shown in Fig. 3 as Δ[Ca], ΔpH, ΔDIC, and $\Delta\Omega_{CaCO_3}$. GRNs have core components that are evolutionarily stable, yet GRNs can also enable marked evolutionary experimentation through the insertion, up-regulation, or silencing of genes or gene clusters (*197*). For example, the formation of the sea urchin spicule within a tubular endothelium is likely a co-optation and repurposing of the same ancestral GRN, vascular endothelial growth factor (VEGF), that forms cylindrical blood vessels in all animals (*46*). There is broad scope for future research in this area, but recent papers by Mass *et al.* (*198*), Ivanina *et al.* (*199*), Herlitze *et al.* (*175*), and Shashikant *et al.* (*200*) show the way forward.

Common protein functions

The extraction and characterization of biomineral-associated proteins have not only revealed notable diversity but also identified commonalities in sequences and functions among protein families and domains (*153*). CA is a ubiquitous biomineralization protein (*107*, *192*), but many other protein classes and functional domains are observed, including tyrosinase, chitin-binding proteins, protease inhibitors, and domains with a typical extracellular matrix signature, such as domains of the Von Willebrand factor, VEGF, or epidermal growth factor (EGF) (*46*, *107*, *153*, *187*, *189*–*193*, *199*, *201*). At the organism level, genomic and transcriptomic studies have revealed numerous protein classes that are associated with biomineralization [e.g., in sea urchins (*195*) and corals (*202*)]. Of these, transmembrane transporter proteins are the best studied, with evidence that biomineralizers use them to transport water, Ca^{2+}, H^+, and bicarbonate anions [corals (*144*) and *Emiliania huxleyi* (*143*)]. Genetic evidence that specific proteins were co-opted for biomineralization or localized within the biomineral or the privileged space is not yet available for many biomineralizing organisms (*202*), but the nonbiomineralizing ancestors of all the phyla that commenced biomineralization in the Ediacaran, Cambrian, and Ordovician Periods very likely had the protein families required for all the functions identified by the integrated model in Fig. 3.

Acidic polymers

Acidic polymers, that is, polysaccharides or proteins containing an abundance of negatively charged functional groups, are a ubiquitous component of marine calcification. Among them, acidic proteins are frequently identified in skeleton-associated proteomes (*203*, *204*). Another notable characteristic ubiquitous in $CaCO_3$ biominerals is the abundance of proteins with low-complexity domains (LCDs) characterized by repetitive sequences of amino acids (*153*, *187*). Thus far, establishing large-scale phylogenies of acidic proteins has been limited (*202*), as these vary widely across lineages. The variability of LCDs suggests that they likely emerged independently within each phylum to perform functions similar across phyla. However, we cannot completely exclude the alternative hypothesis that acidic biomineralizing proteins may have been recruited from ancestral universal calcium-binding intracellular proteins, such as calsequestrins, i.e., proteins of the sarcoplasmic reticulum that exhibit remarkably acidic C termini and can bind numerous calcium ions with a moderate affinity. In coccolithophorids, acidic polysaccharides rather than proteins are extensively associated with the calcitic scales that armor these phytoplankters (*18*). Acidic polymers likely play important chemical roles in biomineralization pathways, including controlling divalent cation activity in the CF (*105*), providing sites for nucleation, coating growth surfaces, and altering the rates of phase transformations (*38*, *205*). We hypothesize that acidic polymers modulate the relative amounts of PA or IA occurring during biomineralization.

Parallel evolution of nacre mesostructure

The independent development of a convergent carbonate mineral structure is elegantly demonstrated by nacre. All three classes of nacre-forming mollusks (bivalves, gastropods, and cephalopods) exhibit GRNs and LCDs. However, a careful examination of nacre-associated protein repertoires indicates either limited homology or no similarity at all (*184*). This strongly suggests that the three major classes of mollusks have evolved nacre biomineralization independently and in parallel (*184*), with the current diversity of nacre proteins reflecting subsequent independent evolution within each lineage. Nacre, however, forms according to the PA + IA model in Fig. 3. Thus, the diversity of nacre proteins suggests evolutionary plasticity, that is, the same functions in the model can be performed in different organisms by different proteins or protein repertoires (*153*).

Insights from the fossil record

The initial diversification of $CaCO_3$ skeletons

The earliest known $CaCO_3$ skeletons are problematic metazoans found in late Ediacaran (550 to 541 Ma before present) rocks distributed globally (*206*–*209*). As noted by Wood (*210*), these fossils are largely confined to coastal carbonate environments where ambient seawater was strongly oversaturated with respect to calcium carbonate minerals, suggesting a limited capacity to modulate fluids within their privileged spaces. By the ensuing Cambrian Period, animals with carbonate skeletons had diversified across a range of shelf and platform environments. Most animal phyla and classes known to form carbonate skeletons started doing so during the Cambrian and Ordovician Periods. From these relatively simple beginnings rooted in widely shared cell biological functionalities, animals evolved the complex biomineralization pathways evident from genomic and proteomic studies [e.g., the work of Jackson *et al.* (*211*)].

Skeletal biomineralization is energetically costly. For example, in corals, the formation of the skeleton and its organic matrix consumes about 30% of the coral's energy budget (*156*, *212*), energy that might otherwise go into reproduction. Thus, for biomineralized skeletons to evolve, the benefits to the organisms must have outweighed their costs. That several clades independently evolved carbonate skeletons at the same time further suggests that diverse organisms responded to some broadly experienced selective pressure. Changes in both the physical and biological environment have been proposed, but the observation that organisms evolved calcium carbonate, silica, phosphate, and agglutinated skeletons in the same time frame strongly implicates predation as a major driver (*213*).

During this Ediacaran-Cambrian interval of skeletal innovation, Earth's oceans shifted from aragonitic to calcitic seas, that is, from waters from which nonskeletal $CaCO_3$ (for example, ooids and seafloor precipitates) formed as aragonite to conditions under which they precipitated as calcite. As first shown by Porter (*176*, *214*) [see also the work of Maloof *et al.* (*215*) and Pruss *et al.* (*216*)], innovations in skeletal mineralization follow the same stratigraphic pattern, with de novo carbonate biomineralization initially favoring aragonite and then, after a literal early Cambrian sea change, calcite in newly evolving groups. This linkage between seawater chemistry and carbonate skeletal innovation persists through several further aragonite-calcite shifts over the past 400 Ma (*217*, *218*).

Skeletons and extinction

$CaCO_3$ biomineralization both reflected and influenced the major diversification events of animals, algae, and other protists. It also influenced the selective sensitivity of different phyla to Earth's great mass extinctions, perhaps especially the largest known extinction at the end of the Permian Period (252 Ma ago). End-Permian catastrophe was triggered by massive volcanism that injected large quantities of CO_2 and other chemicals into the biosphere (*219*), resulting in the intertwined environmental disruptions of global warming, ocean acidification, and deoxygenation of subsurface marine waters (*220*). Experiments motivated by 21st century global change show that different biomineralizing organisms respond in distinct ways to such perturbations (*221*, *222*), corresponding with reasonable accuracy to the selectivity of end-Permian extinctions. On average, calcification in corals and mollusks appears to be particularly vulnerable to the effects of ocean acidification (*223*), especially at the larval stage, whereas arthropods can show increased growth and biomineralization [e.g., the work of Ries *et al.* (*221*)]. At the end of the Permian Period, all calcifying cnidarians disappeared, as did most brachiopod and stalked echinoderm taxa, including most crinoids. Scleractinian corals radiated later, in Triassic oceans, from nonmineralizing sea anemones that survived the end-Permian extinction (*224*). Mollusks showed more moderate levels of extinction, and although some arthropods went extinct (notably the trilobites), others, including the ancestors of decapod crustaceans, not only survived the crisis but also radiated into Mesozoic oceans (*225*). A scenario of volcano-induced environmental change can also be applied to end-Triassic mass extinction (*226*), with similar biological selectivity (*227*), and may help explain other reef crises throughout the Phanerozoic Eon (*228*), including those of the 21st century. Field experiments on the Great Barrier Reef show that carbon dioxide levels predicted for the late 21st century result in substantial reduction of net calcification by entire coral reef ecosystems (*229*, *230*).

There is abundant evidence that different species vary substantially in their responses to ocean acidification (*231*, *232*); this is especially true for corals (*112*, *233*, *234*). Discussions of modern and end-Permian selectivity initially focused on the purported costs of biomineralization in oceans marked by ocean acidification, but experiments by Frieder *et al.* (*235*) and Spalding *et al.* (*236*) indicate that energy limitation is probably not a major source of vulnerability to 21st century or end-Permian environmental change. More likely, differential vulnerabilities relate to the basic physical chemistry of CFs and variations in the capacity of different organisms to modulate CF composition under conditions of ocean acidification, as well as other consequences of rapid pCO_2 increase, including warming and hypercapnia. Consistent with this, some corals are able to modulate pH and calcium in the CFs, minimizing disruption of skeleton accretion under predicted late 21st century conditions (*114*, *132*, *234*).

A key component in predicting the resilience of marine $CaCO_3$ biomineralizers to ocean acidification is understanding the mechanisms involved in biomineralization of the skeletal parts. The model in Fig. 3 highlights that biomineralization never happens in direct contact with seawater but always in privileged compartments. How open to seawater the privileged space is determines how vulnerable to acidification and dissolution each biomineral was, is, or will be in ancient, modern, and future oceans (*68*). Continuing dialog between ancient and modern studies of environmental disruption and its effects on $CaCO_3$ biomineralization promises dividends for both communities, as does the integration of the model in Fig. 3 with evolutionary history.

FUTURE RESEARCH

Improving the model

The interactions between photosynthesis and calcification were not included in the integrated model of Fig. 3, because this review focuses mostly on heterotrophs. These interactions are important today, have been in the fossil record, and would, if included, alter the model of Fig. 3 by adding carbon sources and sinks but would not qualitatively change the biochemical and geochemical networks through which seawater is transformed to carbonate (*29*, *109*, *237*). There is much to be found on the roles that organic matrix macromolecules and ACC play in enabling the formation and functions of biominerals and the consequences of PA of ACC precursors on the elemental and isotopic composition of biominerals (*154*, *155*).

Resilience to climate change

The integrated model and the evolutionary history constrain our understanding of how marine biomineralizers may respond to environmental

change. Although some $CaCO_3$ biomineralizers have proteins that could detect the pH in the ECF (*238*, *239*), it is presently unknown whether organisms achieve homeostasis to an absolute value of ECF chemistry, maintain an offset in solute activities between ECF and seawater, or respond in other ways to seawater chemical fluctuations. These different capabilities make all the difference between continuing and stopping $CaCO_3$ biomineralization in acidifying oceans (*56*). Global climate change is exerting many stressors on marine biomineralizers, and the energy requirement for biomineralization may be a relatively small cost (*236*).

Perhaps the most exciting discoveries ahead will be in elucidating the biomineralization GRNs. For example, they will tell us where key genetic components of the integrated model reside in the genome, in refractory or dynamic regions, and thus whether they are slow or fast in evolving and adapting to changing environments. Evidence for genetic plasticity comes from the observation that several molluscan lineages within cephalopods and gastropods have independently reduced or lost their ancestral $CaCO_3$ shell. These lineages have traits that could be interpreted as effective defenses against predation including, in the case of cephalopods, intelligence, camouflage, fast locomotion, and visual acuity and, in the case of gastropods, toxic or distasteful chemical compounds or sequestration of stinging cells from prey (*240*). These examples suggest that if effective alternative defensive strategies evolve, then the selective pressure of maintaining a calcified shell may be released. It is important to note, however, that most of these lineages do retain the ability to biomineralize $CaCO_3$, and many continue to produce larval shells, internal adult shells, or, in some cases, spicules.

REFERENCES AND NOTES

1. H. A. Lowenstam, Minerals formed by organisms. *Science* **211**, 1126–1131 (1981).
2. H. A. Lowenstam, S. Weiner, *On Biomineralization* (Oxford Univ. Press on Demand, 1989).
3. M. J. Olszta, E. P. Douglas, L. B. Gower, Scanning electron microscopic analysis of the mineralization of type I collagen via a polymer-induced liquid-precursor (PILP) process. *Calcif. Tissue Int.* **72**, 583–591 (2003).
4. S. Mann, Molecular recognition in biomineralization. *Nature* **332**, 119 (1988).
5. L. Li, M. J. Connors, M. Kolle, G. T. England, D. I. Speiser, X. Xiao, J. Aizenberg, C. Ortiz, Multifunctionality of chiton biomineralized armor with an integrated visual system. *Science* **350**, 952–956 (2015).
6. H. Li, C.-Y. Sun, Y. Fang, C. M. Carlson, H. Xu, A. Ješovnik, J. Sosa-Calvo, R. Zarnowski, H. A. Bechtel, J. H. Fournelle, D. R. Andes, T. R. Schultz, P. U. P. A. Gilbert, C. R. Currie, Biomineral armor in leaf-cutter ants. *Nat. Commun.* **11**, 5792 (2020).
7. K. Simkiss, Biomineralization and detoxification. *Calcif. Tissue Res.* **24**, 199–200 (1977).
8. D. H. Erwin, M. Laflamme, S. M. Tweedt, E. A. Sperling, D. Pisani, K. J. Peterson, The Cambrian conundrum: Early divergence and later ecological success in the early history of animals. *Science* **334**, 1091–1097 (2011).
9. A. H. Knoll, S. B. Carroll, Early animal evolution: Emerging views from comparative biology and geology. *Science* **284**, 2129–2137 (1999).
10. A. L. Stigall, R. L. Freeman, C. T. Edwards, C. M. Rasmussen, A multidisciplinary perspective on the Great Ordovician Biodiversification Event and the development of the early Paleozoic world. *Palaeogeogr. Palaeoclimatol. Palaeoecol.* **543**, 109521 (2020).
11. M. Keith, J. Weber, Systematic relationships between carbon and oxygen isotopes in carbonates deposited by modern corals and algae. *Science* **150**, 498–501 (1965).
12. A. Ridgwell, R. E. Zeebe, The role of the global carbonate cycle in the regulation and evolution of the Earth system. *Earth Planet. Sci. Lett.* **234**, 299–315 (2005).
13. S. L. Goldberg, T. M. Present, S. Finnegan, K. D. Bergmann, A high-resolution record of early Paleozoic climate. *Proc. Natl. Acad. Sci. U.S.A.* **118**, (2021).
14. D. H. Erwin, Early metazoan life: Divergence, environment and ecology. *Philos. Trans. R. Soc. Lond. B Biol. Sci.* **370**, 20150036 (2015).
15. P. U. P. A. Gilbert, S. M. Porter, C.-Y. Sun, S. Xiao, B. M. Gibson, N. Shenkar, A. H. Knoll, Biomineralization by particle attachment in early animals. *Proc. Natl. Acad. Sci. U.S.A.* **116**, 17659–17665 (2019).
16. M. S. Clark, Molecular mechanisms of biomineralization in marine invertebrates. *J. Exp. Biol.* **223**, jeb206961 (2020).
17. J. Drake, T. Mass, J. Stołarski, S. Von Euw, B. van de Schootbrugge, P. G. Falkowski, How corals made rocks through the ages. *Glob. Chang. Biol.* **26**, 31–53 (2020).
18. A. R. Taylor, C. Brownlee, G. Wheeler, Coccolithophore cell biology: Chalking up progress. *Ann. Rev. Mar. Sci.* **9**, 283–310 (2017).
19. B. Hönisch, A. Ridgwell, D. N. Schmidt, E. Thomas, S. J. Gibbs, A. Sluijs, R. Zeebe, L. Kump, R. C. Martindale, S. E. Greene, W. Kiessling, J. Ries, J. C. Zachos, D. L. Royer, S. Barker, T. M. Marchitto Jr., R. Moyer, C. Pelejero, P. Ziveri, G. L. Foster, B. Williams, The geological record of ocean acidification. *Science* **335**, 1058–1063 (2012).
20. H. Kawahata, K. Fujita, A. Iguchi, M. Inoue, S. Iwasaki, A. Kuroyanagi, A. Maeda, T. Manaka, K. Moriya, H. Takagi, T. Toyofuku, T. Yoshimura, A. Suzuki, Perspective on the response of marine calcifiers to global warming and ocean acidification—Behavior of corals and foraminifera in a high CO_2 world "hot house". *Prog Earth Planet Sci* **6**, 5 (2019).
21. A. Samperiz, L. F. Robinson, J. A. Stewart, I. Strawson, M. J. Leng, B. E. Rosenheim, E. R. Ciscato, K. R. Hendry, N. Santodomingo, Stylasterid corals: A new paleotemperature archive. *Earth Planet. Sci. Lett.* **545**, 116407 (2020).
22. M. Hermoso, Control of ambient pH on growth and stable isotopes in phytoplanktonic calcifying algae. *Paleoceanography* **30**, 1100–1112 (2015).
23. R. T. DeVol, C.-Y. Sun, M. A. Marcus, S. N. Coppersmith, S. C. B. Myneni, P. U. P. A. Gilbert, Nanoscale transforming mineral phases in fresh nacre. *J. Am. Chem. Soc.* **137**, 13325–13333 (2015).
24. Y. U. T. Gong, C. E. Killian, I. C. Olson, N. P. Appathurai, A. L. Amasino, M. C. Martin, L. J. Holt, F. H. Wilt, P. U. P. A. Gilbert, Phase transitions in biogenic amorphous calcium carbonate. *Proc. Natl. Acad. Sci. U.S.A.* **109**, 6088–6093 (2012).
25. T. Mass, A. J. Giuffre, C.-Y. Sun, C. A. Stifler, M. J. Frazier, M. Neder, N. Tamura, C. V. Stan, M. A. Marcus, P. U. P. A. Gilbert, Amorphous calcium carbonate particles form coral skeletons. *Proc. Natl. Acad. Sci. U.S.A.* **114**, E7670–E7678 (2017).
26. J. J. De Yoreo, P. U. P. A. Gilbert, N. A. J. M. Sommerdijk, R. L. Penn, S. Whitelam, D. Joester, H. Zhang, J. D. Rimer, A. Navrotsky, J. F. Banfield, A. F. Wallace, F. M. Michel, F. C. Meldrum, H. Cölfen, P. M. Dove, Crystallization by particle attachment in synthetic, biogenic, and geologic environments. *Science* **349**, aaa6760 (2015).
27. A. H. Knoll, Biomineralization and evolutionary history, in *Biomineralization*, P. M. Dove, J. J. De Yoreo, S. Weiner, Eds. (Rev Mineral Geochem, Mineral Soc Amer, 2003), vol. 54, pp. 329–356.
28. A. V. Radha, T. Z. Forbes, C. E. Killian, P. U. P. A. Gilbert, A. Navrotsky, Transformation and crystallization energetics of synthetic and biogenic amorphous calcium carbonate. *Proc. Natl. Acad. Sci. U.S.A.* **107**, 16438–16443 (2010).
29. D. E. Jacob, R. Wirth, O. B. A. Agbaje, O. Branson, S. M. Eggins, Planktic foraminifera form their shells via metastable carbonate phases. *Nat. Commun.* **8**, 1265 (2017).
30. L. A. Urry, P. C. Hamilton, C. E. Killian, F. H. Wilt, Expression of spicule matrix proteins in the sea urchin embryo during normal and experimentally altered spiculogenesis. *Dev. Biol.* **225**, 201–213 (2000).
31. D. S. Sevilgen, A. A. Venn, M. Y. Hu, E. Tambutté, D. de Beer, V. Planas-Bielsa, S. Tambutté, Full in vivo characterization of carbonate chemistry at the site of calcification in corals. *Sci. Adv.* **5**, eaau7447 (2019).
32. M. A. Crenshaw, The inorganic composition of molluscan extrapallial fluid. *Biol. Bull.* **143**, 506–512 (1972).
33. E. Beniash, L. Addadi, S. Weiner, Cellular control over spicule formation in sea urchin embryos: A structural approach. *J. Struct. Biol.* **125**, 50–62 (1999).
34. F. H. Wilt, Biomineralization of the spicules of sea urchin embryos. *Zoolog. Sci.* **19**, 253–261 (2002).
35. S. Bentov, C. Brownlee, J. Erez, The role of seawater endocytosis in the biomineralization process in calcareous foraminifera. *Proc. Natl. Acad. Sci. U.S.A.* **106**, 21500–21504 (2009).
36. J. Erez, The source of ions for biomineralization in foraminifera and their implications for paleoceanographic proxies, in *Biomineralization*, P. M. Dove, J. J. De Yoreo, S. Weiner, Eds. (Rev Mineral Geochem, Mineral Soc Amer, 2003), vol. 54, pp. 115–149.
37. J. M. Walker, B. Marzec, N. Ozaki, D. Clare, F. Nudelman, Morphological development of *Pleurochrysis carterae* coccoliths examined by cryo-electron tomography. *J. Struct. Biol.* **210**, 107476 (2020).
38. A. Gal, R. Wirth, J. Kopka, P. Fratzl, D. Faivre, A. Scheffel, Macromolecular recognition directs calcium ions to coccolith mineralization sites. *Science* **353**, 590–593 (2016).
39. B. ter Kuile, J. Erez, The size and function of the internal inorganic carbon pool of the foraminifer *Amphistegina lobifera*. *Mar. Biol.* **99**, 481–487 (1988).
40. B. ter Kuile, J. Erez, E. Padan, Mechanisms for the uptake of inorganic carbon by 2 species of symbiont-bearing foraminifera. *Mar. Biol.* **103**, 241–251 (1989).
41. J. Erez, Vital effect on stable-isotope composition seen in foraminifera and coral skeletons. *Nature* **273**, 199–202 (1978).
42. P. Furla, I. Galgani, I. Durand, D. Allemand, Sources and mechanisms of inorganic carbon transport for coral calcification and photosynthesis. *J. Exp. Biol.* **203**, 3445–3457 (2000).
43. G. M. Khalifa, D. Kirchenbuechler, N. Koifman, O. Kleinerman, Y. Talmon, M. Elbaum, L. Addadi, S. Weiner, J. Erez, Biomineralization pathways in a foraminifer revealed using a novel correlative cryo-fluorescence–SEM–EDS technique. *J. Struct. Biol.* **196**, 155–163 (2016).

44. T. Mass, J. L. Drake, J. M. Heddleston, P. G. Falkowski, Nanoscale visualization of biomineral formation in coral proto-polyps. *Curr. Biol.* **27**, 3191–3196.e3 (2017).
45. N. Vidavsky, S. Addadi, A. Schertel, D. Ben-Ezra, M. Shpigel, L. Addadi, S. Weiner, Calcium transport into the cells of the sea urchin larva in relation to spicule formation. *Proc. Natl. Acad. Sci. U.S.A.* **113**, 12637–12642 (2016).
46. M. Morgulis, T. Gildor, M. Roopin, N. Sher, A. Malik, M. Lalzar, M. Dines, S. B.-T. de-Leon, L. Khalaily, S. B.-T. de-Leon, Possible cooption of a VEGF-driven tubulogenesis program for biomineralization in echinoderms. *Proc. Natl. Acad. Sci. U.S.A.* **116**, 12353–12362 (2019).
47. K. Kahil, N. Varsano, A. Sorrentino, E. Pereiro, P. Rez, S. Weiner, L. Addadi, Cellular pathways of calcium transport and concentration toward mineral formation in sea urchin larvae. *Proc. Natl. Acad. Sci. U.S.A.* **117**, 30957–30965 (2020).
48. C. A. Stifler, C. E. Killian, P. U. P. A. Gilbert, Evidence for a liquid precursor to biomineral formation. *Cryst. Growth Des.* **21**, 6635–6641 (2021).
49. A. Gal, A. Sorrentino, K. Kahil, E. Pereiro, D. Faivre, A. Scheffel, Native-state imaging of calcifying and noncalcifying microalgae reveals similarities in their calcium storage organelles. *Proc. Natl. Acad. Sci. U.S.A.* **115**, 11000–11005 (2018).
50. A. L. Cohen, T. A. McConnaughey, Geochemical perspectives on coral mineralization. *Rev. Mineral. Geochem.* **54**, 151–187 (2003).
51. C.-Y. Sun, C. A. Stifler, R. V. Chopdekar, C. A. Schmidt, G. Parida, V. Schoeppler, B. I. Fordyce, J. H. Brau, T. Mass, S. Tambutté, P. U. P. A. Gilbert, From particle attachment to space-filling coral skeletons. *Proc. Natl. Acad. Sci. U.S.A.* **117**, 30159–30170 (2020).
52. G. Mor Khalifa, S. Levy, T. Mass, The calcifying interface in a stony coral primary polyp: An interplay between seawater and an extracellular calcifying space. *J. Struct. Biol.* **213**, 107803 (2021).
53. C. A. Schmidt, C. A. Stifler, E. L. Luffey, B. I. Fordyce, A. Ahmed, G. Barreiro Pujol, C. P. Breit, S. S. Davison, C. N. Klaus, I. J. Koehler, I. M. LeCloux, C. Matute Diaz, C. M. Nguyen, V. Quach, J. S. Sengkhammee, E. J. Walch, M. M. Xiong, E. Tambutté, S. Tambutté, T. Mass, P. U. P. A. Gilbert, Faster crystallization during coral skeleton formation correlates with resilience to ocean acidification. *J. Am. Chem. Soc.* **144**, 1332–1341 (2022).
54. J. L. Drake, M. F. Schaller, T. Mass, L. Godfrey, A. Fu, R. M. Sherrell, Y. Rosenthal, P. G. Falkowski, Molecular and geochemical perspectives on the influence of CO2 on calcification in coral cell cultures. *Limnol. Oceanogr.* **63**, 107–121 (2018).
55. F. A. Al-Horani, S. M. Al-Moghrabi, D. de Beer, Microsensor study of photosynthesis and calcification in the scleractinian coral, *Galaxea fascicularis*: Active internal carbon cycle. *J. Exp. Mar. Biol. Ecol.* **288**, 1–15 (2003).
56. J. B. Ries, A physicochemical framework for interpreting the biological calcification response to CO2-induced ocean acidification. *Geochim. Cosmochim. Acta* **75**, 4053–4064 (2011).
57. J. Trotter, P. Montagna, M. McCulloch, S. Silenzi, S. Reynaud, G. Mortimer, S. Martin, C. Ferrier-Pagès, J.-P. Gattuso, R. Rodolfo-Metalpa, Quantifying the pH 'vital effect' in the temperate zooxanthellate coral *Cladocora caespitosa*: Validation of the boron seawater pH proxy. *Earth Planet. Sci. Lett.* **303**, 163–173 (2011).
58. M. McCulloch, J. Trotter, P. Montagna, J. Falter, R. Dunbar, A. Freiwald, G. Försterra, M. L. Correa, C. Maier, A. Rüggeberg, Resilience of cold-water scleractinian corals to ocean acidification: Boron isotopic systematics of pH and saturation state up-regulation. *Geochim. Cosmochim. Acta* **87**, 21–34 (2012).
59. Y.-W. Liu, J. N. Sutton, J. B. Ries, R. A. Eagle, Regulation of calcification site pH is a polyphyletic but not always governing response to ocean acidification. *Sci. Adv.* **6**, eaax1314 (2020).
60. P. Ganot, E. Tambutté, N. Caminiti-Segonds, G. Toullec, D. Allemand, S. Tambutté, Ubiquitous macropinocytosis in anthozoans. *eLife* **9**, e50022 (2020).
61. E. Tambutté, S. Tambutté, N. Segonds, D. Zoccola, A. Venn, J. Erez, D. Allemand, Calcein labelling and electrophysiology: Insights on coral tissue permeability and calcification. *Proc. R. Soc. Lond. B Biol. Sci.* **279**, 19–27 (2012).
62. S. Hohn, A. Merico, Quantifying the relative importance of transcellular and paracellular ion transports to coral polyp calcification. *Front. Earth Sci.* **2**, 37 (2015).
63. B. R. Constantz, Coral skeleton construction: A physiochemically dominated process. *PALAIOS* **1**, 152–157 (1986).
64. M. Holcomb, A. Venn, E. Tambutté, S. Tambutté, D. Allemand, J. Trotter, M. McCulloch, Coral calcifying fluid pH dictates response to ocean acidification. *Sci. Rep.* **4**, 5207 (2014).
65. A. C. Gagnon, J. F. Adkins, D. P. Fernandez, L. F. Robinson, Sr/Ca and Mg/Ca vital effects correlated with skeletal architecture in a scleractinian deep-sea coral and the role of Rayleigh fractionation. *Earth Planet. Sci. Lett.* **261**, 280–295 (2007).
66. A. Gal, K. Kahil, N. Vidavsky, R. T. DeVol, P. U. P. A. Gilbert, P. Fratzl, S. Weiner, L. Addadi, Particle accretion mechanism underlies biological crystal growth from an amorphous precursor phase. *Adv. Funct. Mater.* **24**, 5420–5426 (2014).
67. A. Venn, E. Tambutté, M. Holcomb, D. Allemand, S. Tambutté, Live tissue imaging shows reef corals elevate pH under their calcifying tissue relative to seawater. *PLOS ONE* **6**, e20013 (2011).
68. A. A. Venn, C. Bernardet, A. Chabenat, E. Tambutté, S. Tambutté, Paracellular transport to the coral calcifying medium: Effects of environmental parameters. *J. Exp. Biol.* **223**, jeb227074 (2020).
69. N. Vidavsky, S. Addadi, J. Mahamid, E. Shimoni, D. Ben-Ezra, M. Shpigel, S. Weiner, L. Addadi, Initial stages of calcium uptake and mineral deposition in sea urchin embryos. *Proc. Natl. Acad. Sci. U.S.A.* **111**, 39–44 (2014).
70. E. Beniash, J. Aizenberg, L. Addadi, S. Weiner, Amorphous calcium carbonate transforms into calcite during sea urchin larval spicule growth. *Proc. R. Soc. Lond. B Biol. Sci.* **264**, 461–465 (1997).
71. I. M. Weiss, N. Tuross, L. Addadi, S. Weiner, Mollusc larval shell formation: Amorphous calcium carbonate is a precursor phase for aragonite. *J. Exp. Zool.* **293**, 478–491 (2002).
72. Y. Politi, T. Arad, E. Klein, S. Weiner, L. Addadi, Sea urchin spine calcite forms via a transient amorphous calcium carbonate phase. *Science* **306**, 1161–1164 (2004).
73. Y. Politi, R. A. Metzler, M. Abrecht, B. Gilbert, F. H. Wilt, I. Sagi, L. Addadi, S. Weiner, P. U. P. A. Gilbert, Transformation mechanism of amorphous calcium carbonate into calcite in the sea urchin larval spicule. *Proc. Natl. Acad. Sci. U.S.A.* **105**, 17362–17366 (2008).
74. C. E. Killian, R. A. Metzler, Y. T. Gong, I. C. Olson, J. Aizenberg, Y. Politi, F. H. Wilt, A. Scholl, A. Young, A. Doran, M. Kunz, N. Tamura, S. N. Coppersmith, P. U. P. A. Gilbert, The mechanism of calcite co-orientation in the sea urchin tooth. *J. Am. Chem. Soc.* **131**, 18404–18409 (2009).
75. A. B. Rodríguez-Navarro, P. Marie, Y. Nys, M. T. Hincke, J. Gautron, Amorphous calcium carbonate controls avian eggshell mineralization: A new paradigm for understanding rapid eggshell calcification. *J. Struct. Biol.* **190**, 291–303 (2015).
76. M. C. Stoddard, E. H. Yong, D. Akkaynak, C. Sheard, J. A. Tobias, L. Mahadevan, Avian egg shape: Form, function, and evolution. *Science* **356**, 1249–1254 (2017).
77. T. Liberman, A. Genin, Y. Loya, Effects on growth and reproduction of the coral Stylophora pistillata by the mutualistic damselfish *Dascyllus marginatus*. *Mar. Biol.* **121**, 741–746 (1995).
78. M. M. Kotb, Growth rates of three reef-building coral species in the northern Red Sea, Egypt. *Egypt J. Aquat. Biol. Fish.* **5**, 165–185 (2001).
79. L. Shaish, A. Abelson, B. Rinkevich, Branch to colony trajectory in a modular organism: Pattern formation in the Indo-Pacific coral *Stylophora pistillata*. *Dev. Dyn.* **235**, 2111–2121 (2006).
80. E. A. Burton, L. M. Walter, Relative precipitation rates of aragonite and Mg calcite from seawater: Temperature or carbonate ion control? *Geology* **15**, 111–114 (1987).
81. A. Mucci, R. Canuel, S. Zhong, The solubility of calcite and aragonite in sulfate-free seawater and the seeded growth kinetics and composition of the precipitates at 25°C. *Chem. Geol.* **74**, 309–320 (1989).
82. S. Zhong, A. Mucci, Calcite and aragonite precipitation from seawater solutions of various salinities: Precipitation rates and overgrowth compositions. *Chem. Geol.* **78**, 283–299 (1989).
83. A. Gutjahr, H. Dabringhaus, R. Lacmann, Studies of the growth and dissolution kinetics of the $CaCO_3$ polymorphs calcite and aragonite I. Growth and dissolution rates in water. *J. Cryst. Growth* **158**, 296–309 (1996).
84. E. V. Shevchenko, D. V. Talapin, N. A. Kotov, S. O'Brien, C. B. Murray, Structural diversity in binary nanoparticle superlattices. *Nature* **439**, 55 (2006).
85. L. Yang, C. E. Killian, M. Kunz, N. Tamura, P. U. P. A. Gilbert, Biomineral nanoparticles are space-filling. *RSC Nanoscale* **3**, 603–609 (2011).
86. C.-Y. Sun, L. Gránásy, C. A. Stifler, T. Zaquin, R. V. Chopdekar, N. Tamura, J. C. Weaver, J. A. Y. Zhang, S. Goffredo, G. Falini, M. A. Marcus, T. Pusztai, V. Schoeppler, T. Mass, P. U. P. A. Gilbert, Crystal nucleation and growth of spherulites demonstrated by coral skeletons and phase-field simulations. *Acta Biomater.* **120**, 277–292 (2021).
87. I. Polishchuk, A. A. Bracha, L. Bloch, D. Levy, S. Kozachkevich, Y. Etinger-Geller, Y. Kauffmann, M. Burghammer, C. Giacobbe, J. Villanova, G. Hendler, C.-Y. Sun, A. J. Giuffre, M. A. Marcus, L. Kundanati, P. Zaslansky, N. M. Pugno, P. U. P. A. Gilbert, A. Katsman, B. Pokroy, Coherently aligned nanoparticles within a biogenic single crystal: A biological prestressing strategy. *Science* **358**, 1294–1298 (2017).
88. K. T. Faber, A. G. Evans, Crack deflection processes—I. Theory. *Acta Metall.* **31**, 565–576 (1983).
89. M. A. Meyers, J. McKittrick, P.-Y. Chen, Structural biological materials: Critical mechanics-materials connections. *Science* **339**, 773–779 (2013).
90. J. J. De Yoreo, P. M. Dove, Shaping crystals with biomolecules. *Science* **306**, 1301–1302 (2004).
91. A. M. Belcher, X. H. Wu, R. J. Christensen, P. K. Hansma, G. D. Stucky, D. E. Morse, Control of crystal phase switching and orientation by soluble mollusc-shell proteins. *Nature* **381**, 56–58 (1996).
92. G. Falini, S. Albeck, S. Weiner, L. Addadi, Control of aragonite or calcite polymorphism by mollusk shell macromolecules. *Science* **271**, 67–69 (1996).
93. M. Suzuki, K. Saruwatari, T. Kogure, Y. Yamamoto, T. Nishimura, T. Kato, H. Nagasawa, An acidic matrix protein, Pif, is a key macromolecule for nacre formation. *Science* **325**, 1388–1390 (2009).

94. C. Söllner, M. Burghammer, E. Busch-Nentwich, J. Berger, H. Schwarz, C. Riekel, T. Nicolson, Control of crystal size and lattice formation by starmaker in otolith biomineralization. *Science* **302**, 282–286 (2003).
95. T. Mass, J. L. Drake, L. Haramaty, J. D. Kim, E. Zelzion, D. Bhattacharya, P. G. Falkowski, Cloning and characterization of four novel coral acid-rich proteins that precipitate carbonates in vitro. *Curr. Biol.* **23**, 1126–1131 (2013).
96. R. Laipnik, V. Bissi, C.-Y. Sun, G. Falini, P. U. P. A. Gilbert, T. Mass, Coral acid rich protein selects vaterite polymorph in vitro. *J. Struct. Biol.* **209**, 107431 (2020).
97. R. A. Metzler, J. S. Evans, C. E. Killian, D. Zhou, T. H. Churchill, N. P. Appathurai, S. N. Coppersmith, P. U. P. A. Gilbert, Nacre protein fragment templates lamellar aragonite growth. *J. Am. Chem. Soc.* **132**, 6329–6334 (2010).
98. M. P. Mummadisetti, J. L. Drake, P. G. Falkowski, The spatial network of skeletal proteins in a stony coral. *J. R. Soc. Interface* **18**, 20200859 (2021).
99. L. Addadi, S. Weiner, Interactions between acidic proteins and crystals: Stereochemical requirements in biomineralization. *Proc. Natl. Acad. Sci. U.S.A.* **82**, 4110–4114 (1985).
100. X. Yang, D. Yang, Y. Yan, S. Li, Z. Han, Y. Ji, G. Zheng, L. Xie, R. Zhang, A novel matrix protein PfX regulates shell ultrastructure by binding to specific calcium carbonate crystal faces. *Int. J. Biol. Macromol.* **156**, 302–313 (2020).
101. F. Marin, M. Smith, Y. Isa, G. Muyzer, P. Westbroek, Skeletal matrices, muci, and the origin of invertebrate calcification. *Proc. Natl. Acad. Sci. U.S.A.* **93**, 1554–1559 (1996).
102. I. C. Olson, R. A. Metzler, N. Tamura, M. Kunz, C. E. Killian, P. U. P. A. Gilbert, Crystal lattice tilting in prismatic calcite. *J. Struct. Biol.* **183**, 180–190 (2013).
103. A. G. Checa, J. T. Bonarski, M. G. Willinger, M. Faryna, K. Berent, B. Kania, A. González-Segura, C. M. Pina, J. Pospiech, A. Morawiec, Crystallographic orientation inhomogeneity and crystal splitting in biogenic calcite. *J. R. Soc. Interface* **10**, 20130425 (2013).
104. R. A. Metzler, D. Zhou, M. Abrecht, J.-W. Chiou, J. Guo, D. Ariosa, S. N. Coppersmith, P. U. P. A. Gilbert, Polarization-dependent imaging contrast in abalone shells. *Phys. Rev. B* **77**, 064110 (2008).
105. O. Branson, E. A. Bonnin, D. E. Perea, H. J. Spero, Z. Zhu, M. Winters, B. Hönisch, A. D. Russell, J. S. Fehrenbacher, A. C. Gagnon, Nanometer-scale chemistry of a calcite biomineralization template: Implications for skeletal composition and nucleation. *Proc. Natl. Acad. Sci. U.S.A.* **113**, 12934–12939 (2016).
106. D. Bhattacharya, S. Agrawal, M. Aranda, S. Baumgarten, M. Belcaid, J. L. Drake, D. Erwin, S. Foret, R. D. Gates, D. F. Gruber, B. Kamel, M. P. Lesser, O. Levy, Y. J. Liew, M. M. Manes, T. Mass, M. Medina, S. Mehr, E. Meyer, D. C. Price, H. M. Putnam, H. Qiu, C. Shinzato, E. Shoguchi, A. J. Stokes, S. Tambutté, D. Tchernov, C. R. Voolstra, N. Wagner, C. W. Walker, A. P. M. Weber, V. Weis, E. Zelzion, D. Zoccola, P. G. Falkowski, Comparative genomics explains the evolutionary success of reef-forming corals. *eLife* **5**, e13288 (2016).
107. S. Chen, A. C. Gagnon, J. F. Adkins, Carbonic anhydrase, coral calcification and a new model of stable isotope vital effects. *Geochim. Cosmochim. Acta* **236**, 179–197 (2018).
108. V. Raybaud, S. Tambutté, C. Ferrier-Pagès, S. Reynaud, A. A. Venn, É. Tambutté, P. Nival, D. Allemand, Computing the carbonate chemistry of the coral calcifying medium and its response to ocean acidification. *J. Theor. Biol.* **424**, 26–36 (2017).
109. H. L. O. McClelland, J. Bruggeman, M. Hermoso, R. E. M. Rickaby, The origin of carbon isotope vital effects in coccolith calcite. *Nat. Commun.* **8**, 14511 (2017).
110. L. J. de Nooijer, H. Spero, J. Erez, J. Bijma, G.-J. Reichart, Biomineralization in perforate foraminifera. *Earth Sci. Rev.* **135**, 48–58 (2014).
111. A. C. Gagnon, Coral calcification feels the acid. *Proc. Natl. Acad. Sci. U.S.A.* **110**, 1567–1568 (2013).
112. A. A. Venn, E. Tambutte, N. Caminiti-Segonds, N. Techer, D. Allemand, S. Tambutte, Effects of light and darkness on pH regulation in three coral species exposed to seawater acidification. *Sci. Rep.* **9**, 2201 (2019).
113. K. Kahil, S. Weiner, L. Addadi, A. Gal, Ion pathways in biomineralization: Perspectives on uptake, transport, and deposition of calcium, carbonate, and phosphate. *J. Am. Chem. Soc.* **143**, 21100–21112 (2021).
114. A. A. Venn, E. Tambutté, M. Holcomb, J. Laurent, D. Allemand, S. Tambutté, Impact of seawater acidification on pH at the tissue–skeleton interface and calcification in reef corals. *Proc. Natl. Acad. Sci. U.S.A.* **110**, 1634–1639 (2013).
115. S. Ram, J. Erez, The distribution coefficients of major and minor elements in coral skeletons under variable calcium seawater concentrations. *Front. Earth Sci.* **9**, 657176 (2021).
116. Y. Kadan, F. Tollervey, N. Varsano, J. Mahamid, A. Gal, Intracellular nanoscale architecture as a master regulator of calcium carbonate crystallization in marine microalgae. *Proc. Natl. Acad. Sci. U.S.A.* **118**, e2025670118 (2021).
117. S. Kumar, K. Rechav, I. Kaplan-Ashiri, A. Gal, Imaging and quantifying homeostatic levels of intracellular silicon in diatoms. *Sci. Adv.* **6**, eaaz7554 (2020).
118. J. F. Adkins, E. A. Boyle, W. Curry, A. Lutringer, Stable isotopes in deep-sea corals and a new mechanism for "vital effects". *Geochim. Cosmochim. Acta* **67**, 1129–1143 (2003).
119. A. J. Davies, C. M. John, The clumped ($^{13}C^{18}O$) isotope composition of echinoid calcite: Further evidence for "vital effects" in the clumped isotope proxy. *Geochim. Cosmochim. Acta* **245**, 172–189 (2019).
120. A. M. Gothmann, M. L. Bender, C. L. Blättler, P. K. Swart, S. J. Giri, J. F. Adkins, J. Stolarski, J. A. Higgins, Calcium isotopes in scleractinian fossil corals since the Mesozoic: Implications for vital effects and biomineralization through time. *Earth Planet. Sci. Lett.* **444**, 205–214 (2016).
121. M. Hermoso, T. J. Horner, F. Minoletti, R. E. Rickaby, Constraints on the vital effect in coccolithophore and dinoflagellate calcite by oxygen isotopic modification of seawater. *Geochim. Cosmochim. Acta* **141**, 612–627 (2014).
122. A. Katz, M. Bonifacie, M. Hermoso, P. Cartigny, D. Calmels, Laboratory-grown coccoliths exhibit no vital effect in clumped isotope (Δ47) composition on a range of geologically relevant temperatures. *Geochim. Cosmochim. Acta* **208**, 335–353 (2017).
123. A. Meibom, H. Yurimoto, J. P. Cuif, I. Domart-Coulon, F. Houlbreque, B. Constantz, Y. Dauphin, E. Tambutté, S. Tambutté, D. Allemand, J. Wooden, R. Dunbar, Vital effects in coral skeletal composition display strict three-dimensional control. *Geophys. Res. Lett.* **33**, L11608 (2006).
124. C. Saenger, H. P. Affek, T. Felis, N. Thiagarajan, J. M. Lough, M. Holcomb, Carbonate clumped isotope variability in shallow water corals: Temperature dependence and growth-related vital effects. *Geochim. Cosmochim. Acta* **99**, 224–242 (2012).
125. P. T. Spooner, W. Guo, L. F. Robinson, N. Thiagarajan, K. R. Hendry, B. E. Rosenheim, M. J. Leng, Clumped isotope composition of cold-water corals: A role for vital effects? *Geochim. Cosmochim. Acta* **179**, 123–141 (2016).
126. S. Weiner, P. M. Dove, An overview of biomineralization processes and the problem of the vital effect, in *Biomineralization*, P. M. Dove, J. J. De Yoreo, S. Weiner, Eds. (Rev Mineral Geochem, Mineral Soc Amer, 2003), vol. 54, pp. 1–29.
127. N. Allison, D. Chambers, A. A. Finch, Eimf, SIMS sputtering rates in biogenic aragonite: Implications for culture calibration studies for palaeoenvironmental reconstruction. *Surf. Interf. Anal.* **45**, 1389–1394 (2013).
128. M. T. McCulloch, J. P. D'Olivo, J. Falter, L. Georgiou, M. Holcomb, P. Montagna, J. A. Trotter, *Boron Isotopic Systematics in Scleractinian Corals and the Role of pH Up-regulation* (Boron Isotopes, The Fifth Element, 2018), pp. 145–162.
129. M. T. McCulloch, J. P. D'Olivo, J. Falter, M. Holcomb, J. A. Trotter, Coral calcification in a changing world and the interactive dynamics of pH and DIC upregulation. *Nat. Commun.* **8**, 15686 (2017).
130. L. J. de Nooijer, T. Toyofuku, H. Kitazato, Foraminifera promote calcification by elevating their intracellular pH. *Proc. Natl. Acad. Sci. U.S.A.* **106**, 15374–15378 (2009).
131. L. J. de Nooijer, T. Toyofuku, K. Oguri, H. Nomaki, H. Kitazato, Intracellular pH distribution in foraminifera determined by the fluorescent probe HPTS. *Limnol. Oceanogr. Methods* **6**, 610–618 (2008).
132. M. McCulloch, J. Falter, J. Trotter, P. Montagna, Coral resilience to ocean acidification and global warming through pH up-regulation. *Nat. Clim. Chang.* **2**, 623–627 (2012).
133. J. Laurent, S. Tambutté, É. Tambutté, D. Allemand, A. Venn, The influence of photosynthesis on host intracellular pH in scleractinian corals. *J. Exp. Biol.* **216**, 1398–1404 (2013).
134. E. Anagnostou, K.-F. Huang, C.-F. You, E. Sikes, R. Sherrell, Evaluation of boron isotope ratio as a pH proxy in the deep sea coral *Desmophyllum dianthus*: Evidence of physiological pH adjustment. *Earth Planet. Sci. Lett.* **349**, 251–260 (2012).
135. J. A. Stewart, E. Anagnostou, G. L. Foster, An improved boron isotope pH proxy calibration for the deep-sea coral *Desmophyllum dianthus* through sub-sampling of fibrous aragonite. *Chem. Geol.* **447**, 148–160 (2016).
136. T. McConnaughey, ^{13}C and ^{18}O isotopic disequilibrium in biological carbonates: I. Patterns. *Geochim. Cosmochim. Acta* **53**, 151–162 (1989).
137. B. L. Grimm, H. J. Spero, J. M. Harding, T. P. Guilderson, Seasonal radiocarbon reservoir ages for the 17th century James River, Virginia estuary. *Quat. Geochronol.* **41**, 119–133 (2017).
138. H. J. Spero, J. Bijma, D. W. Lea, B. E. Bemis, Effect of seawater carbonate concentration on foraminiferal carbon and oxygen isotopes. *Nature* **390**, 497–500 (1997).
139. J. Lynch-Stieglitz, T. F. Stocker, W. S. Broecker, R. G. Fairbanks, The influence of air-sea exchange on the isotopic composition of oceanic carbon: Observations and modeling. *Global Biogeochem. Cy.* **9**, 653–665 (1995).
140. J. M. Lucas, L. W. Knapp, A physiological evaluation of carbon sources for calcification in the octocoral *Leptogorgia virgulata* (Lamarck). *J. Exp. Biol.* **200**, 2653–2662 (1997).
141. S. Tambutté, E. Tambutté, D. Zoccola, N. Caminiti, S. Lotto, A. Moya, D. Allemand, J. Adkins, Characterization and role of carbonic anhydrase in the calcification process of the azooxanthellate coral *Tubastrea aurea*. *Mar. Biol.* **151**, 71–83 (2007).
142. V. M. Buchsbaum, "Behavioral and physiological responses to light by the sea anemone *Anthopleura elegantissima* as related to its algal endosymbionts," thesis, Stanford University (1968).
143. L. Mackinder, G. Wheeler, D. Schroeder, P. von Dassow, U. Riebesell, C. Brownlee, Expression of biomineralization-related ion transport genes in *Emiliana huxleyi*. *Environ. Microbiol.* **13**, 3250–3265 (2011).
144. D. Zoccola, P. Ganot, A. Bertucci, N. Caminiti-Segonds, N. Techer, C. R. Voolstra, M. Aranda, E. Tambutté, D. Allemand, J. R. Casey, S. Tambutté, Bicarbonate transporters

in corals point towards a key step in the evolution of cnidarian calcification. *Sci. Rep.* **5**, 9983 (2015).
145. V. A. Sleight, P. Antczak, F. Falciani, M. S. Clark, Computationally predicted gene regulatory networks in molluscan biomineralization identify extracellular matrix production and ion transportation pathways. *Bioinformatics* **36**, 1326–1332 (2020).
146. D. V. Dylus, A. Czarkwiani, L. M. Blowes, M. R. Elphick, P. Oliveri, Developmental transcriptomics of the brittle star *Amphiura filiformis* reveals gene regulatory network rewiring in echinoderm larval skeleton evolution. *Genome Biol.* **19**, 26 (2018).
147. E. Usdowski, J. Hoefs, Oxygen isotope exchange between carbonic acid, bicarbonate, carbonate, and water: A re-examination of the data of McCrea (1950) and an expression for the overall partitioning of oxygen isotopes between the carbonate species and water. *Geochim. Cosmochim. Acta* **57**, 3815–3818 (1993).
148. R. E. Zeebe, An explanation of the effect of seawater carbonate concentration on foraminiferal oxygen isotopes. *Geochim. Cosmochim. Acta* **63**, 2001–2007 (1999).
149. C. Saenger, R. I. Gabitov, J. Farmer, J. M. Watkins, R. Stone, Linear correlations in bamboo coral $\delta^{13}C$ and $\delta^{18}O$ sampled by SIMS and micromill: Evaluating paleoceanographic potential and biomineralization mechanisms using $\delta^{11}B$ and Δ_{47} composition. *Chem. Geol.* **454**, 1–14 (2017).
150. L. S. Devriendt, J. M. Watkins, H. V. McGregor, Oxygen isotope fractionation in the CaCO3-DIC-H2O system. *Geochim. Cosmochim. Acta* **214**, 115–142 (2017).
151. J. D. Boettger, J. D. Kubicki, Equilibrium and kinetic isotopic fractionation in the CO_2 hydration and hydroxylation reactions: Analysis of the role of hydrogen-bonding via quantum mechanical calculations. *Geochim. Cosmochim. Acta* **292**, 37–63 (2021).
152. M. Dietzel, B. Purgstaller, T. Kluge, A. Leis, V. Mavromatis, Oxygen and clumped isotope fractionation during the formation of Mg calcite via an amorphous precursor. *Geochim. Cosmochim. Acta* **276**, 258–273 (2020).
153. F. Marin, Mollusc shellomes: Past, present and future. *J. Struct. Biol.* **212**, 107583 (2020).
154. D. Evans, W. R. Gray, J. W. B. Rae, R. Greenop, P. B. Webb, K. Penkman, R. Kröger, N. Allison, Trace and major element incorporation into amorphous calcium carbonate (ACC) precipitated from seawater. *Geochim. Cosmochim. Acta* **290**, 293–311 (2020).
155. C. R. Blue, A. Giuffre, S. Mergelsberg, N. Han, J. J. De Yoreo, P. M. Dove, Chemical and physical controls on the transformation of amorphous calcium carbonate into crystalline $CaCO_3$ polymorphs. *Geochim. Cosmochim. Acta* **196**, 179–196 (2017).
156. A. L. Cohen, M. Holcomb, Why corals care about ocean acidification: Uncovering the mechanism. *Oceanography* **22**, 118–127 (2009).
157. M. Holcomb, A. L. Cohen, R. I. Gabitov, J. L. Hutter, Compositional and morphological features of aragonite precipitated experimentally from seawater and biogenically by corals. *Geochim. Cosmochim. Acta* **73**, 4166–4179 (2009).
158. G. T. Shen, E. A. Boyle, Determination of lead, cadmium and other trace metals in annually-banded corals. *Chem. Geol.* **67**, 47–62 (1988).
159. P. K. Swart, The strontium, magnesium and sodium composition of recent scleractinian coral skeletons as standards for palaeoenvironmental analysis. *Palaeogeogr. Palaeoclimatol. Palaeoecol.* **34**, 115–136 (1981).
160. A. M. Gothmann, J. Stolarski, J. F. Adkins, J. A. Higgins, A Cenozoic record of seawater Mg isotopes in well-preserved fossil corals. *Geology* **45**, 1039–1042 (2017).
161. S. J. Giri, P. K. Swart, Q. B. Devlin, The effect of changing seawater Ca and Mg concentrations upon the distribution coefficients of Mg and Sr in the skeletons of the scleractinian coral *Pocillopora damicornis*. *Geochim. Cosmochim. Acta* **222**, 535–549 (2018).
162. M. E. Gonneea, A. L. Cohen, T. M. DeCarlo, M. A. Charette, Relationship between water and aragonite barium concentrations in aquaria reared juvenile corals. *Geochim. Cosmochim. Acta* **209**, 123–134 (2017).
163. A. Yamazaki, M. Yano, S. Harii, T. Watanabe, Effects of light on the Ba/Ca ratios in coral skeletons. *Chem. Geol.* **559**, 119911 (2021).
164. H. Hauzer, D. Evans, W. Muller, Y. Rosenthal, J. Erez, Calibration of Na partitioning in the calcitic foraminifer *Operculina ammonoides* under variable Ca concentration: Toward reconstructing past seawater composition. *Earth Planet. Sci. Lett.* **497**, 80–91 (2018).
165. E. A. Bonnin, Z. Zhu, J. S. Fehrenbacher, A. D. Russell, B. Hönisch, H. J. Spero, A. C. Gagnon, Submicron sodium banding in cultured planktic foraminifera shells. *Geochim. Cosmochim. Acta* **253**, 127–141 (2019).
166. A. C. Gagnon, J. F. Adkins, J. Erez, Seawater transport during coral biomineralization. *Earth Planet. Sci. Lett.* **329**, 150–161 (2012).
167. A. Roepert, L. Polerecky, E. Geerken, G.-J. Reichart, J. J. Middelburg, Distribution of chlorine and fluorine in benthic foraminifera. *Biogeosciences* **17**, 4727–4743 (2020).
168. D. Evans, W. Müller, J. Erez, Assessing foraminifera biomineralisation models through trace element data of cultures under variable seawater chemistry. *Geochim. Cosmochim. Acta* **236**, 198–217 (2018).
169. F. Bohm, N. Gussone, A. Eisenhauer, W. C. Dullo, S. Reynaud, A. Paytan, Calcium isotope fractionation in modern scleractinian corals. *Geochim. Cosmochim. Acta* **70**, 4452–4462 (2006).
170. N. Gussone, G. Langer, S. Thoms, G. Nehrke, A. Eisenhauer, U. Riebesell, G. Wefer, Cellular calcium pathways and isotope fractionation in *Emiliana huxleyi*. *Geology* **34**, 625–628 (2006).
171. S. T. Mergelsberg, J. J. De Yoreo, Q. R. S. Miller, F. M. Michel, R. N. Ulrich, P. M. Dove, Metastable solubility and local structure of amorphous calcium carbonate (ACC). *Geochim. Cosmochim. Acta* **289**, 196–206 (2020).
172. S. T. Mergelsberg, R. N. Ulrich, S. Xiao, P. M. Dove, Composition systematics in the exoskeleton of the American lobster, *Homarus americanus* and implications for Malacostraca. *Front. Earth Sci.* **7**, 69 (2019).
173. H. Elderfield, C. J. Bertram, J. Erez, Biomineralization model for the incorporation of trace elements into foraminiferal calcium carbonate. *Earth Planet. Sci. Lett.* **142**, 409–423 (1996).
174. T. A. Mashiotta, D. W. Lea, H. J. Spero, Experimental determination of cadmium uptake in shells of the planktonic foraminifera *Orbulina universa* and *Globigerina bulloides*: Implications for surface water paleoreconstructions. *Geochim. Cosmochim. Acta* **61**, 4053–4065 (1997).
175. I. Herlitze, B. Marie, F. Marin, D. J. Jackson, Molecular modularity and asymmetry of the molluscan mantle revealed by a gene expression atlas. *GigaScience* **7**, giy056 (2018).
176. S. Porter, Calcite and aragonite seas and the de novo acquisition of carbonate skeletons. *Geobiology* **8**, 256–277 (2010).
177. C. T. Bolton, H. M. Stoll, Late Miocene threshold response of marine algae to carbon dioxide limitation. *Nature* **500**, 558–562 (2013).
178. M. Hermoso, L. Le Callonnec, F. Minoletti, M. Renard, S. P. Hesselbo, Expression of the early Toarcian negative carbon-isotope excursion in separated carbonate microfractions (Jurassic, Paris Basin). *Earth Planet. Sci. Lett.* **277**, 194–203 (2009).
179. P. U. P. A. Gilbert, K. D. Bergmann, C. E. Myers, M. A. Marcus, R. T. DeVol, C.-Y. Sun, A. Z. Blonsky, E. Tamre, J. Zhao, E. A. Karan, N. Tamura, S. Lemer, A. J. Giuffre, G. Giribet, J. M. Eiler, A. H. Knoll, Nacre tablet thickness records formation temperature in modern and fossil shells. *Earth Planet. Sci. Lett.* **460**, 281–292 (2017).
180. M. Cusack, Y. Dauphin, P. Chung, A. Pérez-Huerta, J.-P. Cuif, Multiscale structure of calcite fibres of the shell of the brachiopod *Terebratulina retusa*. *J. Struct. Biol.* **164**, 96–100 (2008).
181. H. A. Lowenstam, L. Margulis, Evolutionary prerequisites for early Phanerozoic calcareous skeletons. *Biosystems* **12**, 27–41 (1980).
182. E. Sodergren, G. M. Weinstock, E. H. Davidson, R. Andrew Cameron, R. A. Gibbs, R. C. Angerer, L. M. Angerer, M. I. Arnone, D. R. Burgess, R. D. Burke, J. A. Coffman, M. Dean, M. R. Elphick, C. A. Ettensohn, K. R. Foltz, A. Hamdoun, R. O. Hynes, W. H. Klein, W. Marzluff, D. R. McClay, R. L. Morris, A. Mushegian, J. P. Rast, L. Courtney Smith, M. C. Thorndyke, V. D. Vacquier, G. M. Wessel, G. Wray, L. Zhang, C. G. Elsik, O. Ermolaeva, W. Hlavina, G. Hofmann, P. Kitts, M. J. Landrum, A. J. Mackey, D. Maglott, G. Panopoulou, A. J. Poustka, K. Pruitt, V. Sapojnikov, X. Song, A. Souvorov, V. Solovyev, Z. Wei, C. A. Whittaker, K. Worley, K. James Durbin, Y. Shen, O. Fedrigo, D. Garfield, R. Haygood, A. Primus, R. Satija, T. Severson, M. L. Gonzalez-Garay, A. R. Jackson, A. Milosavljevic, M. Tong, C. E. Killian, B. T. Livingston, F. H. Wilt, N. Adams, R. Bellé, S. Carbonneau, R. Cheung, P. Cormier, B. Cosson, J. Croce, A. Fernandez-Guerra, A.-M. Genevière, M. Goel, H. Kelkar, J. Morales, O. Mulner-Lorillon, A. J. Robertson, J. V. Goldstone, B. Cole, D. Epel, B. Gold, M. E. Hahn, M. Howard-Ashby, M. Scally, J. J. Stegeman, E. L. Allgood, J. Cool, K. M. Judkins, S. S. McCafferty, A. M. Musante, R. A. Obar, A. P. Rawson, B. J. Rossetti, I. R. Gibbons, M. P. Hoffman, A. Leone, S. Istrail, S. C. Materna, M. P. Samanta, V. Stolc, W. Tongprasit, Q. Tu, K.-F. Bergeron, B. P. Brandhorst, J. Whittle, K. Berney, D. J. Bottjer, C. Calestani, K. Peterson, E. Chow, Q. A. Yuan, E. Elhaik, D. Graur, J. T. Reese, I. Bosdet, S. Heesun, M. A. Marra, J. Schein, M. K. Anderson, V. Brockton, K. M. Buckley, A. H. Cohen, S. D. Fugmann, T. Hibino, M. Loza-Coll, A. J. Majeske, C. Messier, S. V. Nair, Z. Pancer, D. P. Terwilliger, C. Agca, E. Arboleda, N. Chen, A. M. Churcher, F. Hallböök, G. W. Humphrey, M. M. Idris, T. Kiyama, S. Liang, D. Mellott, X. Mu, G. Murray, R. P. Olinski, F. Raible, M. Rowe, J. S. Taylor, K. Tessmar-Raible, D. Wang, K. H. Wilson, S. Yaguchi, T. Gaasterland, B. E. Galindo, H. J. Gunaratne, C. Juliano, M. Kinukawa, G. W. Moy, A. T. Neill, M. Nomura, M. Raisch, A. Reade, M. M. Roux, J. L. Song, Y.-H. Su, I. K. Townley, E. Voronina, J. L. Wong, G. Amore, M. Branno, E. R. Brown, V. Cavalieri, V. Duboc, L. Duloquin, C. Flytzanis, C. Gache, F. Lapraz, T. Lepage, A. Locascio, P. Martinez, G. Matassi, V. Matranga, R. Range, F. Rizzo, E. Röttinger, W. Beane, C. Bradham, C. Byrum, T. Glenn, S. Hussain, G. Manning, E. Miranda, R. Thomason, K. Walton, A. Wikramanayake, S.-Y. Wu, R. Xu, C. Titus Brown, L. Chen, R. F. Gray, P. Y. Lee, J. Nam, P. Oliveri, J. Smith, D. Muzny, S. Bell, J. Chacko, A. Cree, S. Curry, C. Davis, H. Dinh, S. Dugan-Rocha, J. Fowler, R. Gill, C. Hamilton, J. Hernandez, S. Hines, J. Hume, L. Jackson, A. Jolivet, C. Kovar, S. Lee, L. Lewis, G. Miner, M. Morgan, L. V. Nazareth, G. Okwuonu, D. Parker, L.-L. Pu, R. Thorn, R. Wright, The genome of the sea urchin *Strongylocentrotus purpuratus*. *Science* **314**, 941–952 (2006).
183. B. T. Livingston, C. E. Killian, F. Wilt, A. Cameron, M. J. Landrum, O. Ermolaeva, V. Sapojnikov, D. R. Maglott, A. M. Buchanan, C. A. Ettensohn, A genome-wide analysis

of biomineralization-related proteins in the sea urchin *Strongylocentrotus purpuratus*. *Dev. Biol.* **300**, 335–348 (2006).
184. D. J. Jackson, C. McDougall, B. Woodcroft, P. Moase, R. A. Rose, M. Kube, R. Reinhardt, D. S. Rokhsar, C. Montagnani, C. Joubert, D. Piquemal, B. M. Degnan, Parallel evolution of nacre building gene sets in molluscs. *Mol. Biol. Evol.* **27**, 591–608 (2010).
185. B. Marie, C. Joubert, A. Tayalé, I. Zanella-Cléon, C. Belliard, D. Piquemal, N. Cochennec-Laureau, F. Marin, Y. Gueguen, C. Montagnani, Different secretory repertoires control the biomineralization processes of prism and nacre deposition of the pearl oyster shell. *Proc. Natl. Acad. Sci. U.S.A.* **109**, 20986–20991 (2012).
186. J. Germer, K. Mann, G. Wörheide, D. J. Jackson, The skeleton forming proteome of an early branching metazoan: A molecular survey of the biomineralization components employed by the coralline sponge *Vaceletia* sp. *PLOS ONE* **10**, e0140100 (2015).
187. K. M. Kocot, F. Aguilera, C. McDougall, D. J. Jackson, B. M. Degnan, Sea shell diversity and rapidly evolving secretomes: Insights into the evolution of biomineralization. *Front. Zool.* **13**, 23 (2016).
188. J. Arivalagan, T. Yarra, B. Marie, V. A. Sleight, E. Duvernois-Berthet, M. S. Clark, A. Marie, S. Berland, Insights from the shell proteome: Biomineralization to adaptation. *Mol. Biol. Evol.* **34**, 66–77 (2017).
189. K. Mann, N. Cerveau, M. Gummich, M. Fritz, M. Mann, D. J. Jackson, In-depth proteomic analyses of *Haliotis laevigata* (greenlip abalone) nacre and prismatic organic shell matrix. *Proteome Sci.* **16**, 11 (2018).
190. A. H. Knoll, Biomineralization and evolutionary history. *Rev. Mineral. Geochem.* **54**, 329–356 (2003).
191. L. Addadi, D. Joester, F. Nudelman, S. Weiner, Mollusk shell formation: A source of new concepts for understanding biomineralization processes. *Chem. A Eur. J.* **12**, 980–987 (2006).
192. N. Le Roy, D. J. Jackson, B. Marie, P. Ramos-Silva, F. Marin, The evolution of metazoan α-carbonic anhydrases and their roles in calcium carbonate biomineralization. *Front. Zool.* **11**, 75 (2014).
193. D. J. E. Murdock, The 'biomineralization toolkit' and the origin of animal skeletons. *Biol. Revs.* **95**, 1372–1392 (2020).
194. D. J. Jackson, B. M. Degnan, The importance of evo-devo to an integrated understanding of molluscan biomineralisation. *J. Struct. Biol.* **196**, 67–74 (2016).
195. K. Rafiq, T. Shashikant, C. J. McManus, C. A. Ettensohn, Genome-wide analysis of the skeletogenic gene regulatory network of sea urchins. *Development* **141**, 950–961 (2014).
196. S. Ben-Tabou de-Leon, E. H. Davidson, Gene regulation: Gene control network in development. *Annu. Rev. Biophys. Biomol. Struct.* **36**, 191–212 (2007).
197. E. H. Davidson, D. H. Erwin, Gene regulatory networks and the evolution of animal body plans. *Science* **311**, 796–800 (2006).
198. T. Mass, H. M. Putnam, J. L. Drake, E. Zelzion, R. D. Gates, D. Bhattacharya, P. G. Falkowski, Temporal and spatial expression patterns of biomineralization proteins during early development in the stony coral *Pocillopora damicornis*. *Proc. R. Soc. Lond. B Biol. Sci.* **283**, 20160322 (2016).
199. A. V. Ivanina, B. Borah, T. Rimkevicius, J. Macrander, H. Piontkivska, I. M. Sokolova, E. Beniash, The role of the vascular endothelial growth factor (VEGF) signaling in biomineralization of the oyster *Crassostrea gigas*. *Front. Mar. Sci.* **5**, 309 (2018).
200. T. Shashikant, J. M. Khor, C. A. Ettensohn, From genome to anatomy: The architecture and evolution of the skeletogenic gene regulatory network of sea urchins and other echinoderms. *Genesis* **56**, e23253 (2018).
201. P. Ramos-Silva, J. Kaandorp, L. Huisman, B. Marie, I. Zanella-Cléon, N. Guichard, D. J. Miller, F. Marin, The skeletal proteome of the coral *Acropora millepora*: The evolution of calcification by co-option and domain shuffling. *Mol. Biol. Evol.* **30**, 2099–2112 (2013).
202. T. Zaquin, A. Malik, J. L. Drake, H. M. Putnam, T. Mass, Evolution of protein-mediated biomineralization in scleractinian corals. *Front. Genet.* **12**, 618517 (2021).
203. J. L. Drake, T. Mass, L. Haramaty, E. Zelzion, D. Bhattacharya, P. G. Falkowski, Proteomic analysis of skeletal organic matrix from the stony coral *Stylophora pistillata*. *Proc. Natl. Acad. Sci. U.S.A.* **110**, 3788–3793 (2013).
204. B.-A. Gotliv, N. Kessler, J. L. Sumerel, D. E. Morse, N. Tuross, L. Addadi, S. Weiner, Asprich: A novel aspartic acid-rich protein family from the prismatic shell matrix of the bivalve *Atrina rigida*. *Chembiochem* **6**, 304–314 (2005).
205. L. Addadi, J. Moradian, E. Shay, N. G. Maroudas, S. Weiner, A chemical model for the cooperation of sulfates and carboxylates in calcite crystal nucleation: Relevance to biomineralization. *Proc. Natl. Acad. Sci. U.S.A.* **84**, 2732–2736 (1987).
206. G. J. Germs, New shelly fossils from Nama Group, South West Africa. *Am. J. Sci.* **272**, 752–761 (1972).
207. S. W. Grant, Shell structure and distribution of *Cloudina*, a potential index fossil for the terminal Proterozoic. *Am. J. Sci.* **290**, 261–294 (1990).
208. J. P. Grotzinger, W. A. Watters, A. H. Knoll, Calcified metazoans in thrombolite-stromatolite reefs of the terminal Proterozoic Nama Group, Namibia. *Paleobiology* **26**, 334–359 (2000).
209. R. A. Wood, J. P. Grotzinger, J. Dickson, Proterozoic modular biomineralized metazoan from the Nama Group, Namibia. *Science* **296**, 2383–2386 (2002).
210. R. A. Wood, Paleoecology of the earliest skeletal metazoan communities: Implications for early biomineralization. *Earth Sci. Rev.* **106**, 184–190 (2011).
211. D. J. Jackson, S. M. Degnan, B. M. Degnan, Variation in rates of early development in *Haliotis asinina* generate competent larvae of different ages. *Front. Zool.* **9**, 2 (2012).
212. D. Allemand, É. Tambutté, D. Zoccola, S. Tambutté, Coral calcification, cells to reefs, in *Coral Reefs: An Ecosystem in Transition* (Springer, 2011), pp. 119–150.
213. S. Bengtson, *Early Cambrian Fossils from South Australia* (Association of Australasian Palaeontologists, 1990), vol. 9, pp. 364.
214. S. M. Porter, Seawater chemistry and early carbonate biomineralization. *Science* **316**, 1302–1302 (2007).
215. A. C. Maloof, S. M. Porter, J. L. Moore, F. Ö. Dudás, S. A. Bowring, J. A. Higgins, D. A. Fike, M. P. Eddy, The earliest Cambrian record of animals and ocean geochemical change. *GSA Bull.* **122**, 1731–1774 (2010).
216. S. B. Pruss, S. Finnegan, W. W. Fischer, A. H. Knoll, Carbonates in skeleton-poor seas: New insights from Cambrian and Ordovician strata of Laurentia. *PALAIOS* **25**, 73–84 (2010).
217. S. M. Stanley, L. A. Hardie, Secular oscillations in the carbonate mineralogy of reef-building and sediment-producing organisms driven by tectonically forced shifts in seawater chemistry. *Palaeogeogr. Palaeoclimatol. Palaeoecol.* **144**, 3–19 (1998).
218. W. Kiessling, M. Aberhan, L. Villier, Phanerozoic trends in skeletal mineralogy driven by mass extinctions. *Nat. Geosci.* **1**, 527–530 (2008).
219. S. D. Burgess, S. Bowring, S.-Z. Shen, High-precision timeline for Earth's most severe extinction. *Proc. Natl. Acad. Sci. U.S.A.* **111**, 3316–3321 (2014).
220. A. H. Knoll, R. K. Bambach, J. L. Payne, S. Pruss, W. W. Fischer, Paleophysiology and end-Permian mass extinction. *Earth Planet. Sci. Lett.* **256**, 295–313 (2007).
221. J. B. Ries, A. L. Cohen, D. C. McCorkle, Marine calcifiers exhibit mixed responses to CO_2-induced ocean acidification. *Geology* **37**, 1131–1134 (2009).
222. F. Melzner, M. Gutowska, M. Langenbuch, S. Dupont, M. Lucassen, M. Thorndyke, M. Bleich, H.-O. Pörtner, Physiological basis for high CO_2 tolerance in marine ectothermic animals: Pre-adaptation through lifestyle and ontogeny? *Biogeosciences* **6**, 2313–2331 (2009).
223. K. J. Kroeker, R. L. Kordas, R. Crim, I. E. Hendriks, L. Ramajo, G. S. Singh, C. M. Duarte, J. P. Gattuso, Impacts of ocean acidification on marine organisms: Quantifying sensitivities and interaction with warming. *Glob. Chang. Biol.* **19**, 1884–1896 (2013).
224. A. M. Quattrini, E. Rodríguez, B. C. Faircloth, P. F. Cowman, M. R. Brugler, G. A. Farfan, M. E. Hellberg, M. V. Kitahara, C. L. Morrison, D. A. Paz-García, D. A. Paz-García, J. D. Reimer, C. S. McFadden, Palaeoclimate ocean conditions shaped the evolution of corals and their skeletons through deep time. *Nat. Ecol. Evol.* **4**, 1531–1538 (2020).
225. C. E. Schweitzer, R. M. Feldmann, The Decapoda (Crustacea) as predators on Mollusca through geologic time. *PALAIOS* **25**, 167–182 (2010).
226. B. Schoene, J. Guex, A. Bartolini, U. Schaltegger, T. J. Blackburn, Correlating the end-Triassic mass extinction and flood basalt volcanism at the 100 ka level. *Geology* **38**, 387–390 (2010).
227. W. Kiessling, M. Aberhan, B. Brenneis, P. J. Wagner, Extinction trajectories of benthic organisms across the Triassic–Jurassic boundary. *Palaeogeogr. Palaeoclimatol. Palaeoecol.* **244**, 201–222 (2007).
228. W. Kiessling, C. Simpson, On the potential for ocean acidification to be a general cause of ancient reef crises. *Glob. Chang. Biol.* **17**, 56–67 (2011).
229. R. Albright, L. Caldeira, J. Hosfelt, L. Kwiatkowski, J. K. Maclaren, B. M. Mason, Y. Nebuchina, A. Ninokawa, J. Pongratz, K. L. Ricke, T. Rivlin, K. Schneider, M. Sesboüé, K. Shamberger, J. Silverman, K. Wolfe, K. Zhu, K. Caldeira, Reversal of ocean acidification enhances net coral reef calcification. *Nature* **531**, 362–365 (2016).
230. B. D. Eyre, T. Cyronak, P. Drupp, E. H. De Carlo, J. P. Sachs, A. J. Andersson, Coral reefs will transition to net dissolving before end of century. *Science* **359**, 908–911 (2018).
231. S. Widdicombe, J. I. Spicer, Predicting the impact of ocean acidification on benthic biodiversity: What can animal physiology tell us? *J. Exp. Mar. Biol. Ecol.* **366**, 187–197 (2008).
232. A. H. Knoll, W. W. Fischer, J. Gattuso, L. Hansson, Skeletons and ocean chemistry: The long view, in *Ocean Acidification*, J. P. Gattuso, L. Hansson, Eds. (Oxford University Press, 2011), vol. 4, pp. 67–82.
233. M. K. Morikawa, S. R. Palumbi, Using naturally occurring climate resilient corals to construct bleaching-resistant nurseries. *Proc. Natl. Acad. Sci. U.S.A.* **116**, 10586–10591 (2019).
234. T. M. De Carlo, S. Comeau, C. E. Cornwall, M. T. McCulloch, Coral resistance to ocean acidification linked to increased calcium at the site of calcification. *Proc. R. Soc. Lond. B Biol. Sci.* **285**, 20180564 (2018).
235. C. A. Frieder, S. L. Applebaum, T.-C. F. Pan, D. Hedgecock, D. T. Manahan, Metabolic cost of calcification in bivalve larvae under experimental ocean acidification. *ICES J. Mar. Sci.* **74**, 941–954 (2017).
236. C. Spalding, S. Finnegan, W. W. Fischer, Energetic costs of calcification under ocean acidification. *Global Biogeochem. Cycles* **31**, 866–877 (2017).

237. M. Inoue, T. Nakamura, Y. Tanaka, A. Suzuki, Y. Yokoyama, H. Kawahata, K. Sakai, N. Gussone, A simple role of coral-algal symbiosis in coral calcification based on multiple geochemical tracers. *Geochim. Cosmochim. Acta* **235**, 76–88 (2018).
238. A. R. Taylor, A. Chrachri, G. Wheeler, H. Goddard, C. Brownlee, A voltage-gated H+ channel underlying pH homeostasis in calcifying coccolithophores. *PLoS Biol.* **9**, e1001085 (2011).
239. K. L. Barott, A. A. Venn, A. B. Thies, S. Tambutté, M. Tresguerres, Regulation of coral calcification by the acid-base sensing enzyme soluble adenylyl cyclase. *Biochem. Biophys. Res. Commun.* **525**, 576–580 (2020).
240. H. Wägele, A. Klussmann-Kolb, Opisthobranchia (Mollusca, Gastropoda)–more than just slimy slugs. Shell reduction and its implications on defence and foraging. *Front. Zool.* **2**, 3 (2005).
241. K. D. Bergmann, N. Boekelheide, A shift from equilibrium: Analysis of isotopic variability across modern biomineralizing organisms (OSF, 2021); https://osf.io/rvc58/.
242. A. Ernst, Diversity dynamics of Ordovician bryozoa. *Lethaia* **51**, 198–206 (2018).
243. A. P. Ippolitov, O. Vinn, E. K. Kupriyanova, M. Jäger, Written in stone: History of serpulid polychaetes through time. *Mem. Mus. Vic.* **71**, 123–160 (2014).
244. A. Kouchinsky, S. Bengtson, B. Runnegar, C. Skovsted, M. Steiner, M. Vendrasco, Chronology of early Cambrian biomineralization. *Geol. Mag.* **149**, 221–251 (2012).
245. J. Vinther, P. Van Roy, D. E. G. Briggs, Machaeridians are Palaeozoic armoured annelids. *Nature* **451**, 185–188 (2008).
246. J. Wendt, The first tunicate with a calcareous exoskeleton (Upper Triassic, northern Italy). *Palaeontology* **61**, 575–595 (2018).
247. J. Erez, The source of ions for biomineralization in foraminifera and their implications for paleoceanographic proxies. *Rev. Mineral. Geochem.* **54**, 115–149 (2003).
248. J. W. B. Rae, Boron isotopes in foraminifera: Systematics, biomineralisation, and CO_2 reconstruction, in *Boron Isotopes* (Springer, 2018), pp. 107–143.

Acknowledgments: We thank the Radcliffe Institute for Advanced Study at Harvard University for funding and hosting the workshop "Biomineralization: integrating mechanism and evolutionary history" on 11 and 12 July 2019. All coauthors of this paper participated in intense discussions for 2 days in person and 2 years by email to achieve consensus. Thus, this paper is the direct result of that workshop. Thank you, Radcliffe! **Author contributions:** Conceptualization: P.U.P.A.G. and A.H.K. Methodology: P.U.P.A.G., K.D.B., and A.H.K. Meta-analysis: K.D.B. and N.B. Consensus model development: All coauthors. Writing—original draft: P.U.P.A.G., K.D.B., and A.H.K. Writing—review and editing: All coauthors. **Competing interests:** The authors declare that they have no financial or other competing interests. **Data and materials availability:** All data needed to evaluate the conclusions in the paper, including the complete meta-analysis of carbon and oxygen isotope data and code, are available in the public domain on https://osf.io/rvc58/ and cited as (*241*).

Submitted 17 August 2021
Accepted 6 January 2022
Published 9 March 2022
10.1126/sciadv.abl9653

Biomineralization: Integrating mechanism and evolutionary history

Pupa U. P. A. GilbertKristin D. BergmannNicholas BoekelheideSylvie TambutténTali MassFrédéric MarinJess F. AdkinsJonathan ErezBenjamin GilbertVanessa KnutsonMarjorie CantineJavier Ortega HernándezAndrew H. Knoll

Sci. Adv., 8 (10), eabl9653. • DOI: 10.1126/sciadv.abl9653